NASA CR-132749

EFFECT OF PRECIPITATION ON CHOICE OF FREQUENCY FOR SEASAT SCATTEROMETER

CRES Technical Report 186-14

George Dome

July 1975

Supported by:

National Aeronautics and Space Administration
Langley Research Center
Hampton, Virginia 23365

Contract NAS 1-10048

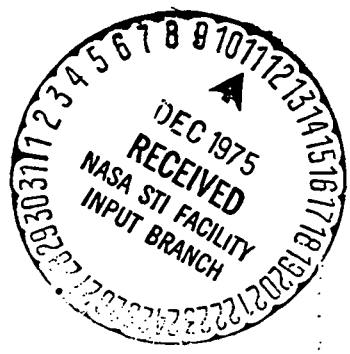

THE UNIVERSITY OF KANSAS CENTER FOR RESEARCH, INC.
2385 Irving Hill Drive—Campus West Lawrence, Kansas 66045

ABSTRACT

Errors in measuring wind speed with radar backscatter from the sea occur due to precipitation backscatter. The return power during precipitation consists of returns from both the ocean and the precipitation. This combination of ocean and precipitation returns causes an inaccurate estimate of the radar cross section of the sea, σ^{o}, which results in an inaccurate estimate of the wind speed.

Calculations were made at three frequencies considered possible for the SEASAT scatterometer: 12.5, 13.9, and 15 GHz. The wind response of σ^{o} is slightly stronger at higher frequencies; and the backscatter and attenuation caused by rain is less troublesome at lower frequencies. Representative errors at cell 7 of the proposed SEASAT system (at f = 13.9 GHz) are: (1) With vertical polarization the user's requirement, wind speed measurement precision to within $\pm$ 2 m/sec or $\pm$ 10% whichever is greater, is violated for wind speeds above 45 knots for rain rate = 2.8 mm/hr. and wind speeds of 5 - 6 knots; those above 31 knots for rain rate = 5.2 mm/hr, and wind speeds of 5 - 9 knots; and those above 24 knots for rain rate = 10.3 mm/hr. (2) For horizontal polarization the user's requirement is violated at wind speeds of 5 - 9 knots for rain rate = 2.8 mm/hr, wind speeds of 5 - 15 knots and those above 40 knots for rain rate = 2.8 mm/hr, and wind speeds of 5 - 17.5 knots and those above 32 knots for rain rate = 10.3 mm/hr.

1. INTRODUCTION

Precipitation backscatter limits the effectiveness of a remote sensing radar in a satellite. Scatterometer operation on SEASAT is being considered in one of the following frequency ranges: (1) 12.5 GHz, (2) 13.4 - 14.0 GHz, or 14.4 - 15.35 GHz. This study compares the effect of backscatter from precipitation in these frequency ranges.

In deciding on a frequency not only should the backscatter from precipitation be considered, but also the dependence of σ^o on frequency. The higher the operating frequency the more dependent σ^o becomes on wind speed. Combining the studies on backscatter from precipitation vs. frequency, and σ^o vs. frequency should make it possible to decide on a frequency best suited for the study of sea conditions.

2. PRECIPITATION EFFECTS

Precipitation will affect the accuracy of the σ^o measurement, and thus that of the wind speed in each of the proposed frequency ranges. To determine the extent of the error induced by precipitation, two factors must be considered: (1) precipitation backscatter and (2) attenuation due to precipitation. Therefore, a model for precipitation must be used to yield realistic results.

Very little is known about the vertical distributions of rain over the ocean. Consequently, we must assume that rainfall distribution over the ocean is the same as over land. This report limits itself to a single rainfall case out of the many possible. The rainfall case[3] is that of a summer rain in temperate latitude or if the temperature were slightly higher, of widespread tropical rains. Using three different updrafts, it is possible to determine three different precipitation rates.

CASE 1: 0.4 m/sec updraft
rain: $0 \leq z \leq 3100$ m, $r = 10.3$ mm/hr
cloud: $3100 \text{ m} \leq z \leq 7000$ m, $M = 0.3$ gm/m^3

CASE 2: 0.2 m/sec updraft
rain: $0 \leq z \leq 3300$ m, $r = 5.2$ mm/hr
cloud: $3300 \leq z \leq 7000$ m, $M = 0.15$ gm/m^3

CASE 3: 0.1 m/sec updraft
rain: $0 \leq z \leq 3500$ m, $r = 2.8$ mm/hr
cloud: 3500 m $\leq z \leq$ 7000 m, $M = 0.1$ gm/m^3

Since vertical extent of rain over the ocean is usually less than in the model, this represents a conservative model.

Because rain is not uniform, a limitation on the extent of precipitation is needed in the model. James [4] determined that in Eastern England the horizontal extent of precipitation can be given by,

Precipitation extent, (d) = 41.4 - 23.5 log r, (km).

While the "James Model" is certainly inappropriate for a tropical rain storm, adequate models of horizontal extent of rain are not well documented, so this one is used.

Using the horizontal extent of precipitation, d, along with the cell width ℓ (see Appendix 1) the maximum area of precipitation is

$$\text{Precipitation Area}_{max.} = d \times \ell$$

(shown in Figure 1). Combining this with the vertical extent of precipitation, z, the maximum volume of precipitation is simply

$$\text{Precipitation Volume}_{max} = z \times d \times \ell .$$

Table 1 contains the maximum values of precipitation area and volume for cells 1, 3, 7, 12 of the proposed SEASAT scatterometer using the precipitation rates assumed by our model.

2.1 Radar Return From Precipitation

The return power from precipitation can be obtained from the familiar radar equation,

$$W_r = W_t \frac{G^2 \lambda^2 \sigma L}{(4\pi)^3 R^4} \qquad (1)$$

where

W_t = transmitted power
G = antenna gain (G^2, since we assume that the same antenna is used for both transmitting and receiving)

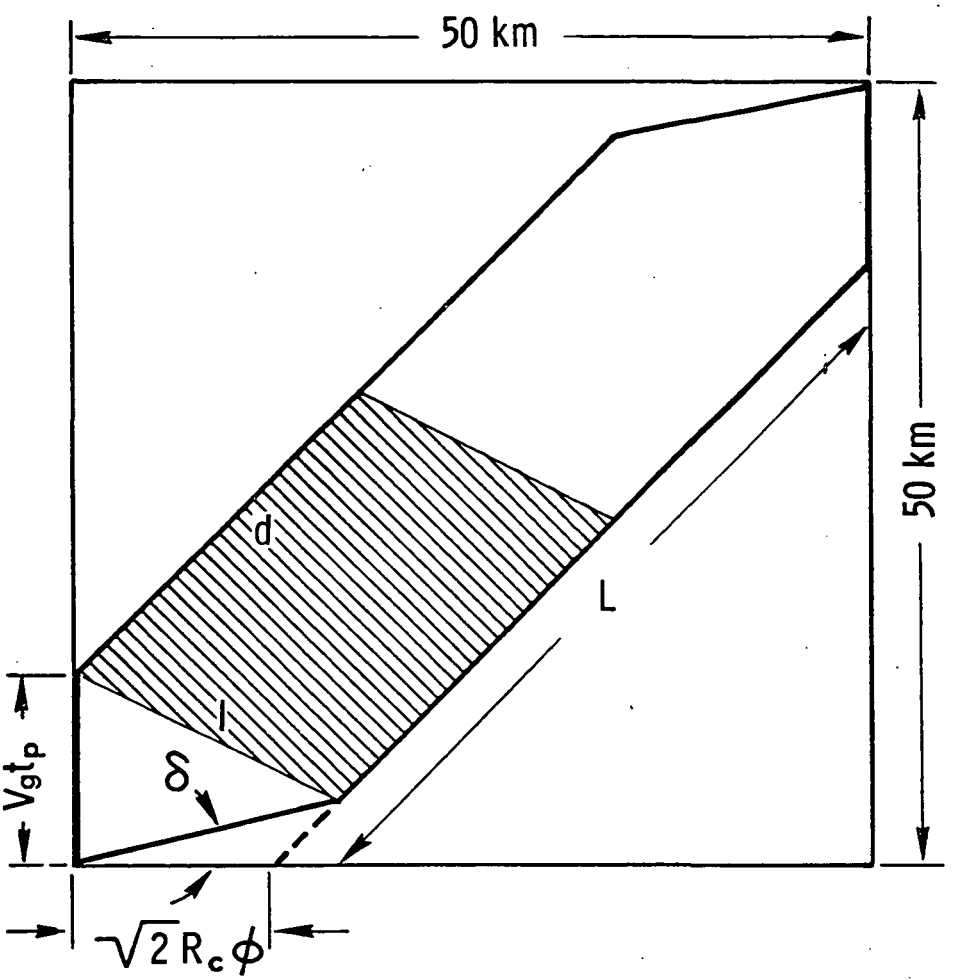

Figure 1. Resolution Cell.

Table 1: Maximum area and volume of precipitation for cells 1, 3, 7, 12

Cell #	Rainfall Rate (mm/hr)	Area of Precipitation (km^2)	Path Length in Precipitation (Average) (Km)	Volume (km^3)
1	10.3	290.93	3.327	901.88
	7.9	335.56	3.435	1073.79
	5.2	406.14	3.542	1340.26
	2.8	510.61	3.757	1787.13
3	10.3	300.78	3.548	932.42
	7.9	346.93	3.662	1110.18
	5.2	419.90	3.777	1385.67
	2.8	527.91	4.006	1847.68
7	10.3	329.47	4.109	1021.36
	7.9	380.02	4.241	1216.04
	5.2	459.95	4.374	1517.83
	2.8	578.26	4.639	2023.91
12	10.3	378.05	4.864	1171.95
	7.9	436.04	5.021	1395.33
	5.2	527.76	5.178	1741.61
	2.8	663.52	5.492	2322.32

R = range

L = loss factor

λ = wavelength

σ = radar cross section.

The radar cross section of precipitation can be though of as a volume resolution cell containing many independent scatterers each with a cross section of σ ;

$$\sigma = V_m \sum_i \sigma_i \tag{2}$$

where V_m is the volume of the resolution cell.

The expression for the radar cross section of a single spherical drop, σ , was developed by Mie,[1]

$$\sigma_i = \frac{\pi a^2}{\alpha^2} \left| \sum_n (-1)^n (2n + 1)(a_n - b_n) \right|^2 \tag{3}$$

where a is the drop radius, $\alpha = 2\pi a/\lambda$, and a_n, b_n "are coefficients in the expression for the scattered field; the a_n terms refer to the scattering arising from the induced magnetic dipole, quadrupole, etc.; and the b_n terms refer to the electric dipole, quadrupole, etc."[1] Assuming $a < \lambda$, this can be given by the approximation,

$$\sigma_i = \frac{64\pi^5}{\lambda^4} |K|^2 a_i^6 \tag{4a}$$

or by

$$\sigma_i = \frac{\pi^5}{\lambda^4} |K|^2 D_i^6 \tag{4b}$$

where D_i is the drop diameter. The value of $|K|^2$ is given by (5),

$$K = \frac{m^2 - 1}{m^2 + 1} \tag{5}$$

where $m = n - jK$. The parameters n, K are determined by the following relationships[2]

TABLE 2. Determination of $|K|^2$ as a function of frequency at 20°C.

FREQUENCY (GHz)	WAVELENGTH (cm)	x	m = n - jK	K^2
12.2	2.4590	0.6209	7.9820 - j2.0936	0.9264
12.5	2.4000	0.6362	7.9442 - j2.1260	0.9263
13.4	2.2388	0.6820	7.8306 - j2.2167	0.9260
13.6	2.2059	0.6921	7.8054 - j2.2356	0.9260
13.8	2.1739	0.7023	7.7800 - j2.2543	0.9259
14.0	2.1429	0.7125	7.7545 - j2.2725	0.9258
14.4	2.0833	0.7329	7.7037 - j2.3079	0.9257
14.6	2.0548	0.7430	7.6785 - j2.3249	0.9256
14.8	2.0270	0.7532	7.6530 - j2.3416	0.9255
15.0	2.0000	0.7634	7.6275 - j2.3580	0.9255
15.2	1.9737	0.7736	7.6022 - j2.3739	0.9254
15.35	1.9544	0.7812	7.5832 - j2.3857	0.9253

Table 3: Two-way transmission loss (attenuation) due to precipitation

Precipitation Rate (mm/hr) / Cell #	10.3	7.9	5.2	2.8
	Attenuation (dB), Frequency = 12.5 GHz			
1	2.29	1.71	1.05	0.526
3	2.44	1.82	1.12	0.561
7	2.83	2.11	1.30	0.649
12	3.35	2.50	1.54	0.769

Precipitation Rate (mm/hr) / Cell #	10.3	7.9	5.2	2.8
	Attenuation (dB), Frequency = 13.9 GHz			
1	2.71	2.05	1.29	0.661
3	2.89	2.18	1.37	0.705
7	3.34	2.53	1.59	0.816
12	3.96	2.99	1.88	0.966

Table 3: (cont'd.)

Precipitation Rate (mm/hr) / Cell #	10.3	7.9	5.2	2.8
	Attenuation (dB), Frequency = 15.0 GHz			
1	3.19	2.42	1.54	0.796
3	3.40	2.58	1.64	0.849
7	3.94	2.98	1.90	0.983
12	4.66	3.53	2.25	1.16

$$n = \frac{1}{\sqrt{2}} \left\{ \sqrt{\frac{\epsilon_s^2 + \epsilon_o^2 \chi^2}{1 + \chi^2}} + \frac{\epsilon_s + \epsilon_o \chi^2}{1 + \chi^2} \right\}^{1/2} \tag{6}$$

$$jK = \frac{1}{\sqrt{2}} \left\{ \sqrt{\frac{\epsilon_s^2 + \epsilon_o^2 \chi^2}{1 + \chi^2}} - \frac{\epsilon_s + \epsilon_o \chi^2}{1 + \chi^2} \right\}^{1/2} \tag{7}$$

$$\chi = \frac{2\pi \times 3 \times 10^{10}}{\lambda} \tau_o \tag{8}$$

where for 20°C, $\epsilon_o = 5.5$, $\tau_o = 8.1 \times 10^{-12}$, $\epsilon_s = 80.08$. Table 2 shows values of $|K|^2$ for the frequencies of interest. This parameter will be assumed constant over the frequency range of interest, $|K|^2 = 0.926$.

Letting L, the loss factor, consist only of attenuation from precipitation, an expression for L can be obtained from an empirical expression first proposed by Gunn and East,

$$L = A = aR^b \tag{9}$$

where

A = attenuation (dB/km)

R = rainfall rate (mm/hr)

a & b = frequency dependent constants.

Assuming a Laws and Parson distribution, the parameters a and b [9] for the three frequencies of interest are

12.5 GHz: a = 0.20, b = 1.22

13.9 GHz: a = 0.26, b = 1.18

15.0 GHz: a = 0.032, b = 1.16.

Using the values above for a and b, the two-way transmission loss due to precipitation is given in Table 3.

The values given in Table 3 are for the two-way transmission of the signal through the rain to the ground and back. For precipitation echoes, the attenuation is about one-half the value given in Table 3, since the average path length through the rain is one-half the complete distance to the ground.

Thus, the return from precipitation can be given by

$$W_{rp} = \frac{W_t G^2 \lambda^2 L}{(4\pi)^3 R^4} V_m \sum_i \frac{\pi^5}{\lambda^4} |K|^2 D_i^6$$

$$= \frac{W_t G^2 L_\pi^2 |K|^2}{64 \lambda^2 R^4} V_m \sum_i D_i^2 \qquad (10)$$

For continuous rain $\sum_i D_i^6$ is given by Z where $Z = 200r^{1.6}$ (mm^6/m^3). Therefore the return power from precipitation becomes

$$W_{rp} = \frac{W_t G^2 L\pi^2 |K|^2}{64 \lambda^2 R^4} V_m(200r^{1.6}) \qquad (11)$$

3.0 RADAR RETURN FROM THE OCEAN

At the frequencies of interest, the major scattering surface is the capillary waves. This can be shown by considering Bragg's resonance condition; according to the Bragg resonance condition, the radar return will be governed by ocean waves of wavelength Γ which satisfy

$$\Gamma = \frac{n\lambda}{2 \sin \theta} \qquad (12)$$

where

λ = wavelength

n = order of resonance

θ = incident angle.

Knowing that the capillary wave spectrum governs the scattering, the scattering coefficient can be determined from small perturbation theory:

$$\sigma_{vv}^0 (\theta) = \frac{8\pi}{k^4} \cos^4 \theta |R_{vv}|^2 S(2k \sin \theta) \qquad (13)$$

$$\sigma^{\circ}_{HH}(\theta) = \frac{8\pi}{k^4} \cos^4 \theta |R_{HH}|^2 S(2k \sin \theta) \tag{14}$$

where

$S(2k \sin \theta)$ = capillary spectrum

R_{VV}, R_{HH} = the Fresnel coefficient in the horizontal and vertical planes, respectively

k = radar wave number

θ = incident angle.

This result appears satisfactory for vertical polarization, since composite surface scattering theories indicate that the long wavelength components have negligible effect on the scattering. Unfortunately, this is not the case for horizontal polarizations. The tilting of the larger wavelength structure influences the reflectivity and thus, the small perturbation theory is not as valid. This should be remembered when comparing theoretical and SKYLAB results.

The Fresnel coefficients for both the horizontal and vertical planes are given by the following expressions,

$$R_{VV} = \frac{\varepsilon_r \cos \theta - \sqrt{\varepsilon_r - \sin^2 \theta}}{\varepsilon_r \cos \theta + \sqrt{\varepsilon_r - \sin^2 \theta}} \tag{15}$$

$$R_{HH} = \frac{\cos \theta - \sqrt{\varepsilon_r - \sin^2 \theta}}{\cos \theta + \sqrt{\varepsilon_r - \sin^2 \theta}} \tag{16}$$

where ϵ_r is the complex relative dielectric constant of sea water. Using Porter's work[7], the complex relative dielectric constant, ϵ_r, is given by

$$\varepsilon_r = \varepsilon_r' - j\varepsilon_r'' \tag{17}$$

$$\varepsilon_r' = 4.8 + \frac{(\varepsilon_s - 4.8)\left[1 + \left(\frac{\lambda_s}{\lambda}\right)^{0.98} (\pi \times 10^{-2})\right]}{1 + 2\left(\frac{\lambda_s}{\lambda}\right)^{0.98} (\pi \times 10^{-2}) + (\lambda_s/\lambda)^{1.96}} \tag{18}$$

$$\varepsilon_r'' = \frac{(\varepsilon_s - 4.8)(\lambda_s/\lambda)^{0.98}}{1 + 2(\lambda_s/\lambda)^{0.98}(\pi \times 10^{-2}) + (\lambda_s/\lambda)^{1.96}} + \frac{18\sigma}{f} \qquad (19)$$

The parameters are:

ϵ_s = $87.8 - 15.3N - 0.363T$

λ_s = $3.38 - 0.11T + 0.00147T^2 + 0.0173TN - 0.52N$

σ = $5n + 0.12TN + 0.04T$

λ = wavelength (cm)

f = frequency (GHz)

N = normality = salinity / 58.45

T = temperature (°C)

Pierson[5] proposes the following expression for the capillary spectrum when the friction velocity is greater than 12 cm/sec,

$$S(2k \sin\theta) = \frac{1.3(2\pi)^{P-1}(g + 3gK^2/13.18)}{K(gK + gK^3/13.18)^{(P+1)/2}} F(\psi) \qquad (20)$$

where

P = $5.29 - 1.176 \log_{10} u_*$

u_* = friction velocity (cm/sec)

g = gravitation constant (981 ergs)

K = ocean wave number. In this case K set = $2k \sin\theta$

$F(\Psi)$ = angular spectrum ($\frac{1}{\pi}$ [$1 + 0.78 \cos 2\Psi$])

Thus, a theoretical value for σ° can be obtained by specifying frequency, polarization, wind speed and incident angle. Theoretical values for σ° at frequencies and incident angles of interest are given in Figures 2, 3 and 4.

Figure 2: (a) σ_{VV}° (30°) vs. wind speed
(b) σ_{HH}° (30°) vs. wind speed

Figure 3: (a) σ_{VV}° (40°) vs. wind speed
(b) σ_{HH}° (40°) vs. wind speed

Figure 4: (a) σ_{VV}° (50°) vs. wind speed
(b) σ_{HH}° (50°) vs. wind speed

A comparison can be made between theoretical and measured values of $\sigma_{vv}^{\circ}(\theta)$ and $\sigma_{HH}^{\circ}(\theta)$. Preliminary results from SKYLAB are given in Figures 5, 6 and 7.

Figure 5: (a) σ_{vv}° (30°) vs. wind speed
(b) σ_{HH}° (30°) vs. wind speed

Figure 6: (a) σ_{vv}° (40°) vs. wind speed
(b) σ_{HH}° (40°) vs. wind speed

Figure 7: (a) σ_{vv}° (50°) vs. wind speed
(b) σ_{HH}° (50°) vs. wind speed

The theoretical value of σ° appears to be a few dB higher than that measured by SKYLAB (but Pierson has since modified his expression for the capillary spectrum).

With the value of σ° known, the return signal power, W_{rs}, can be obtained by the radar equation. Substituting $\sigma = \sigma^{\circ}A$ into the radar equation yields

$$W_{rs} = \frac{W_t G^2 \lambda^2 L \sigma^{\circ} A}{(4\pi)^3 R^4} \tag{22}$$

The value of A is derived in Appendix 1 for cells 1, 3, 7 and 12. In this analysis, the value of L is given in Table 3.*

4.0 EFFECT OF PRECIPITATION ON WIND SPEED MEASUREMENTS

A plot of σ° vs. wind speed on log-log paper suggests a power law relationship of the form

$$\sigma^{\circ} = AU^{\gamma}$$
$$\sigma^{\circ}(\text{dB}) = A(\text{dB}) + \gamma(10 \log_{10} U) \tag{23}$$

*The values for the remaining variables were obtained from "An Operational Satellite Scatterometer For Wind Vector Measurements Over the Ocean," a working document at Langley Research Center.

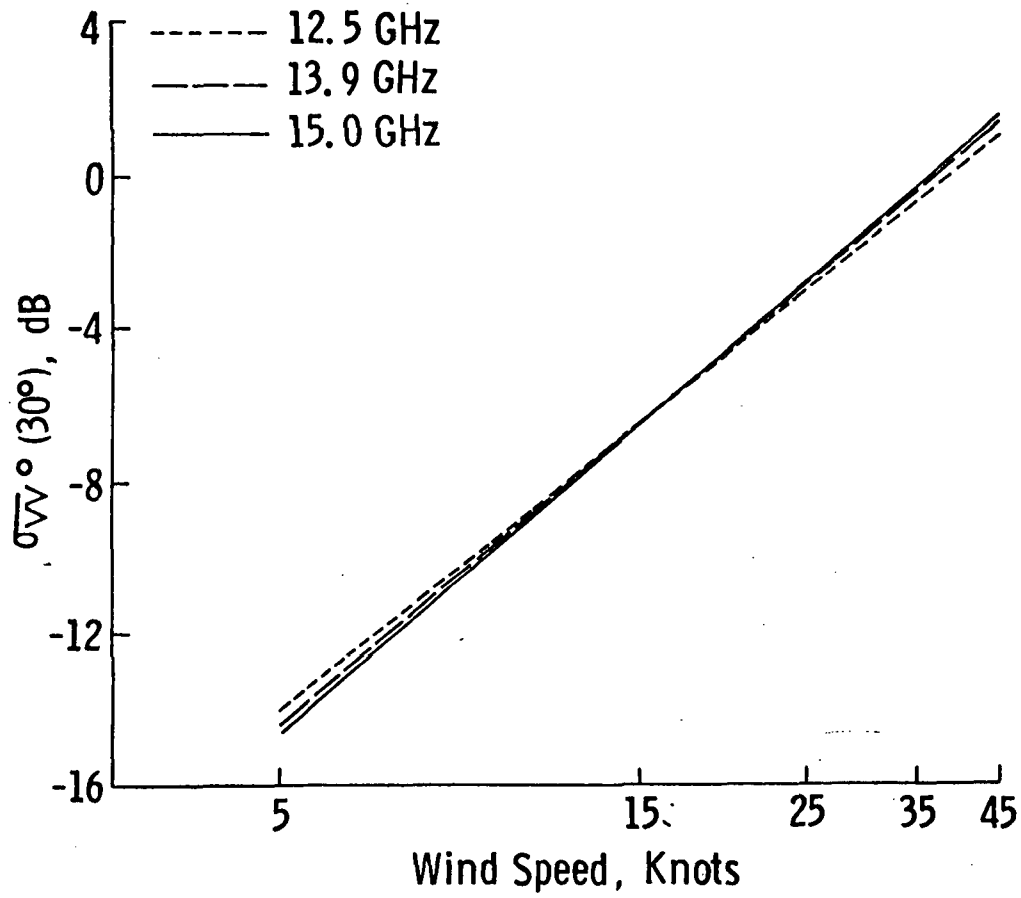

Figure 2a. Radar cross section, σ_{VV}° (30°) vs. wind speed.

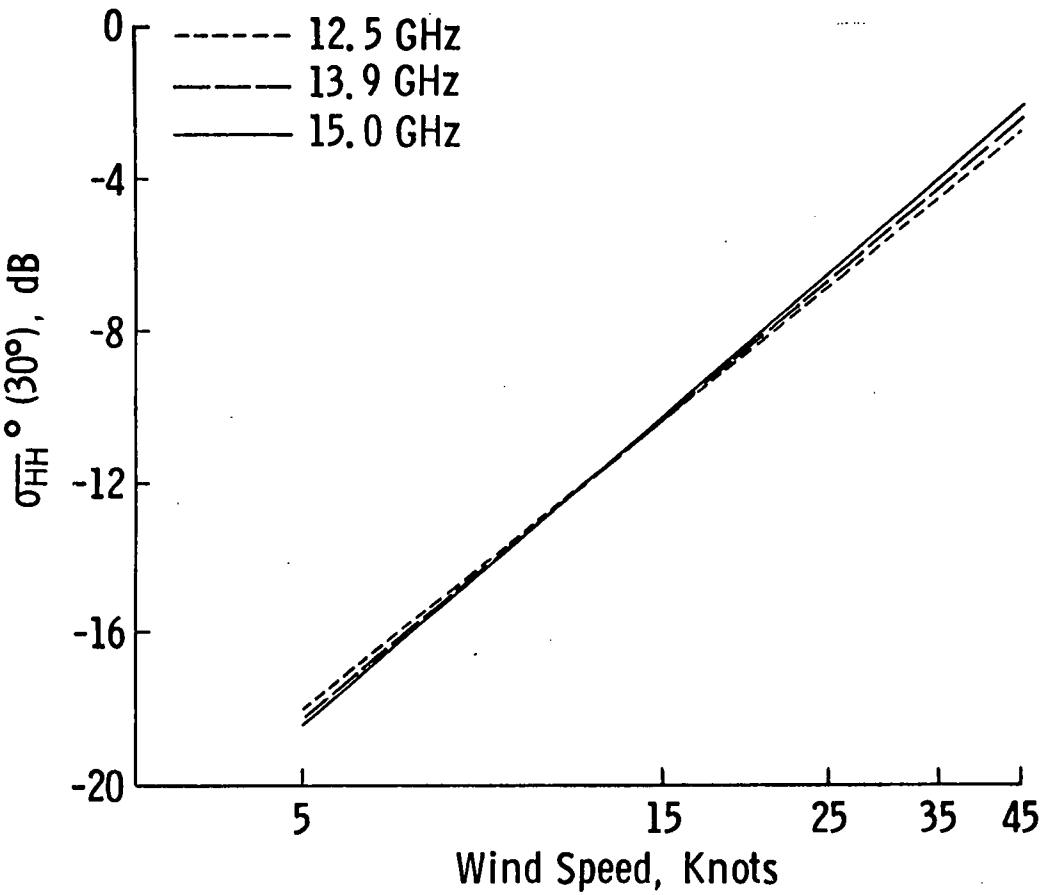

Figure 2b. Radar cross section, $\overline{\sigma_{HH}}^{\circ}(30^{\circ})$ vs. wind speed.

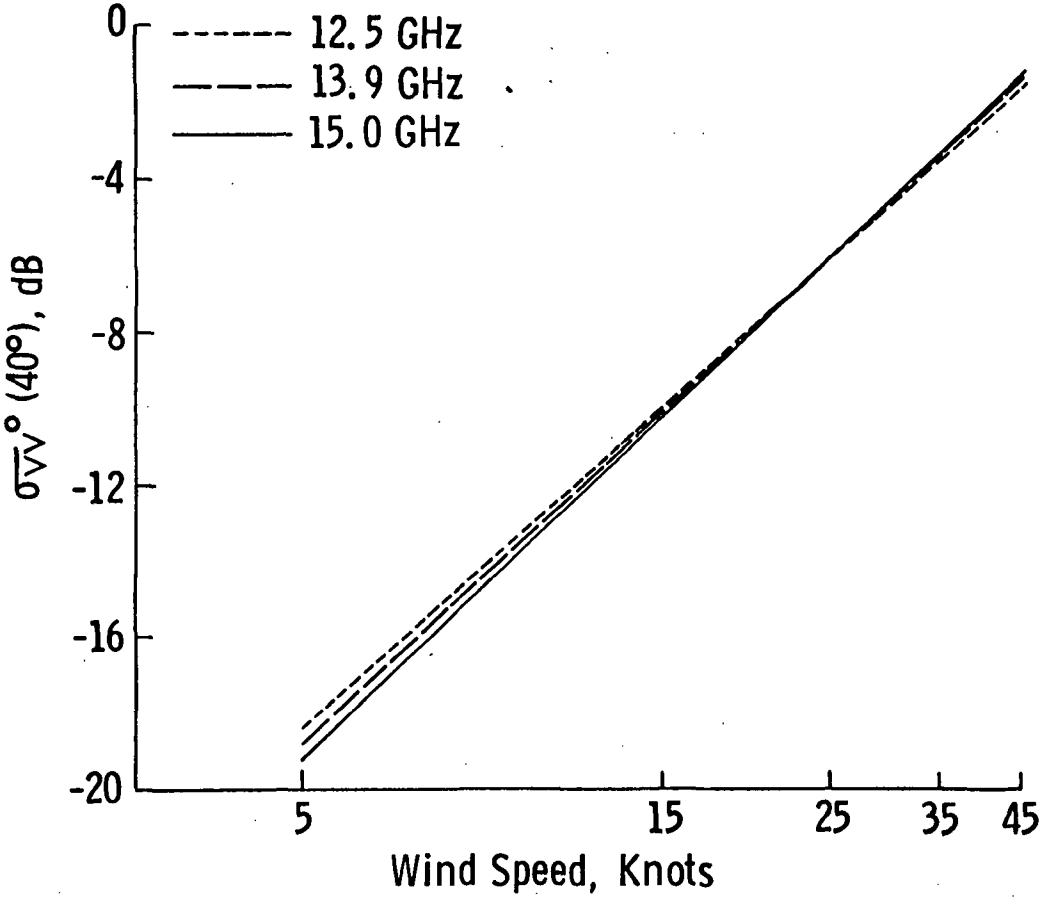

Figure 3a. Radar cross section, $\overline{\sigma_{VV}}^{\circ}$ (40°) vs. wind speed.

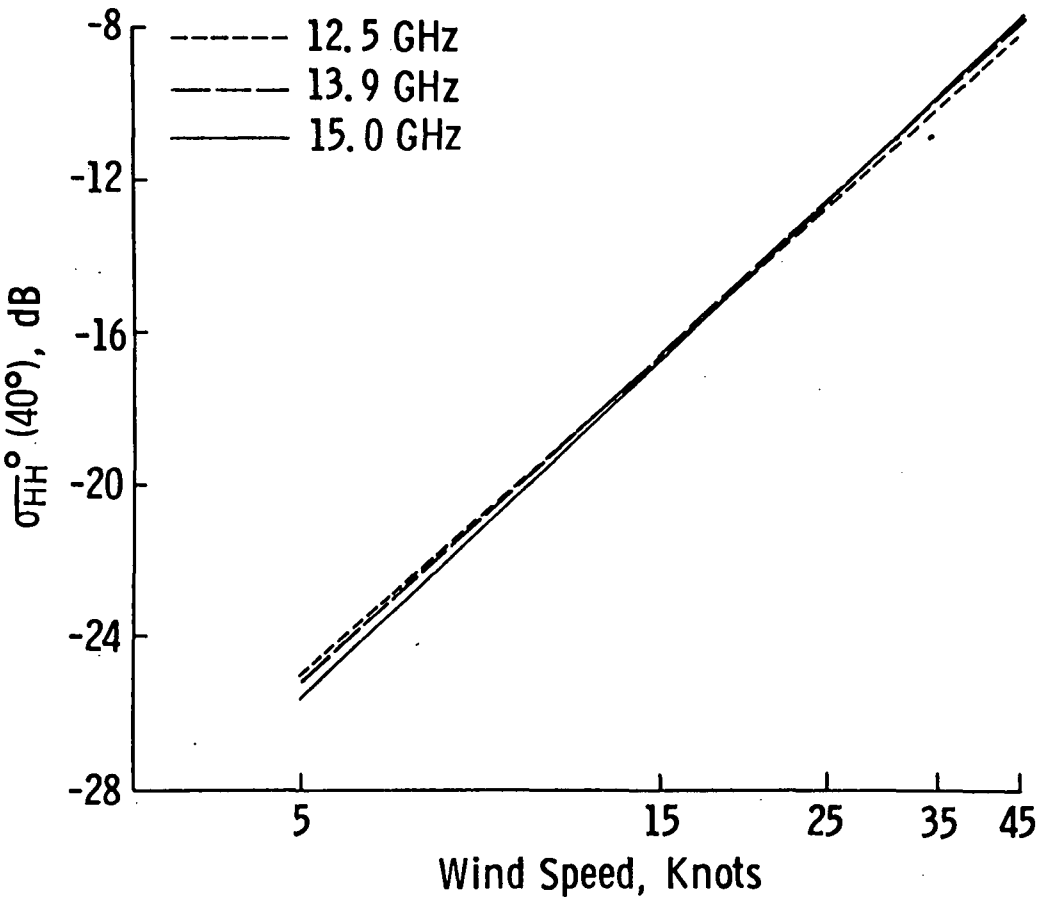

Figure 3b. Radar cross section, $\overline{\sigma_{HH}}^{\circ}(40^{\circ})$ vs. wind speed.

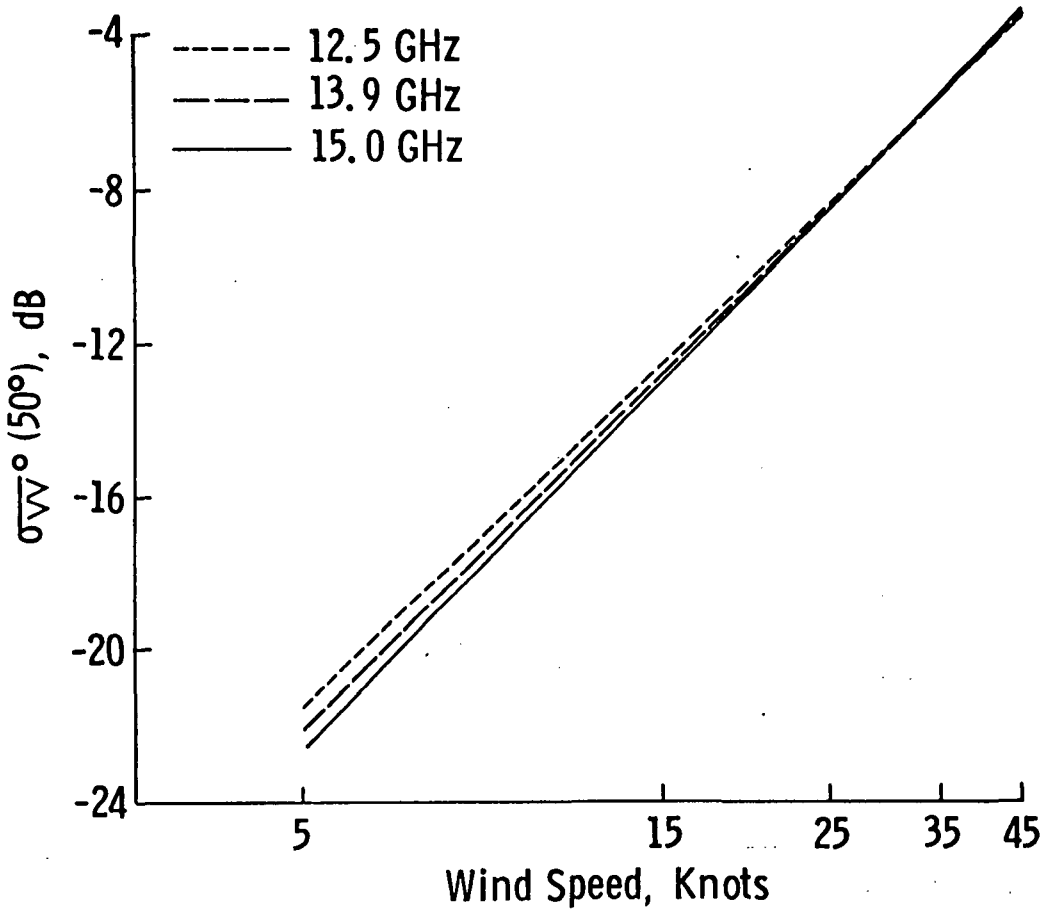

Figure 4a. Radar cross section, σ_{VV}° (50°) vs. wind speed.

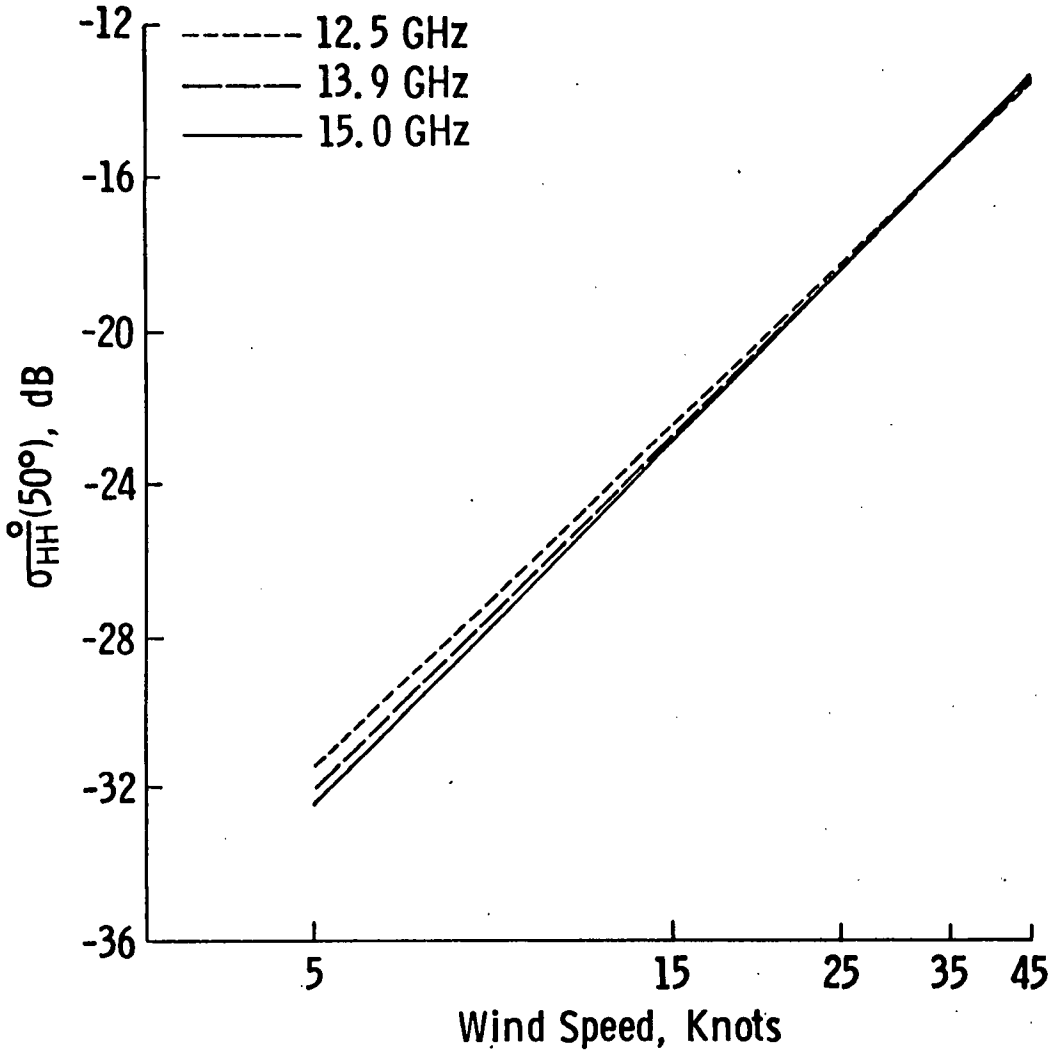

Figure 4b. Radar cross section, $\overline{\sigma_{HH}^{\circ}}(50^{\circ})$ vs. wind speed.

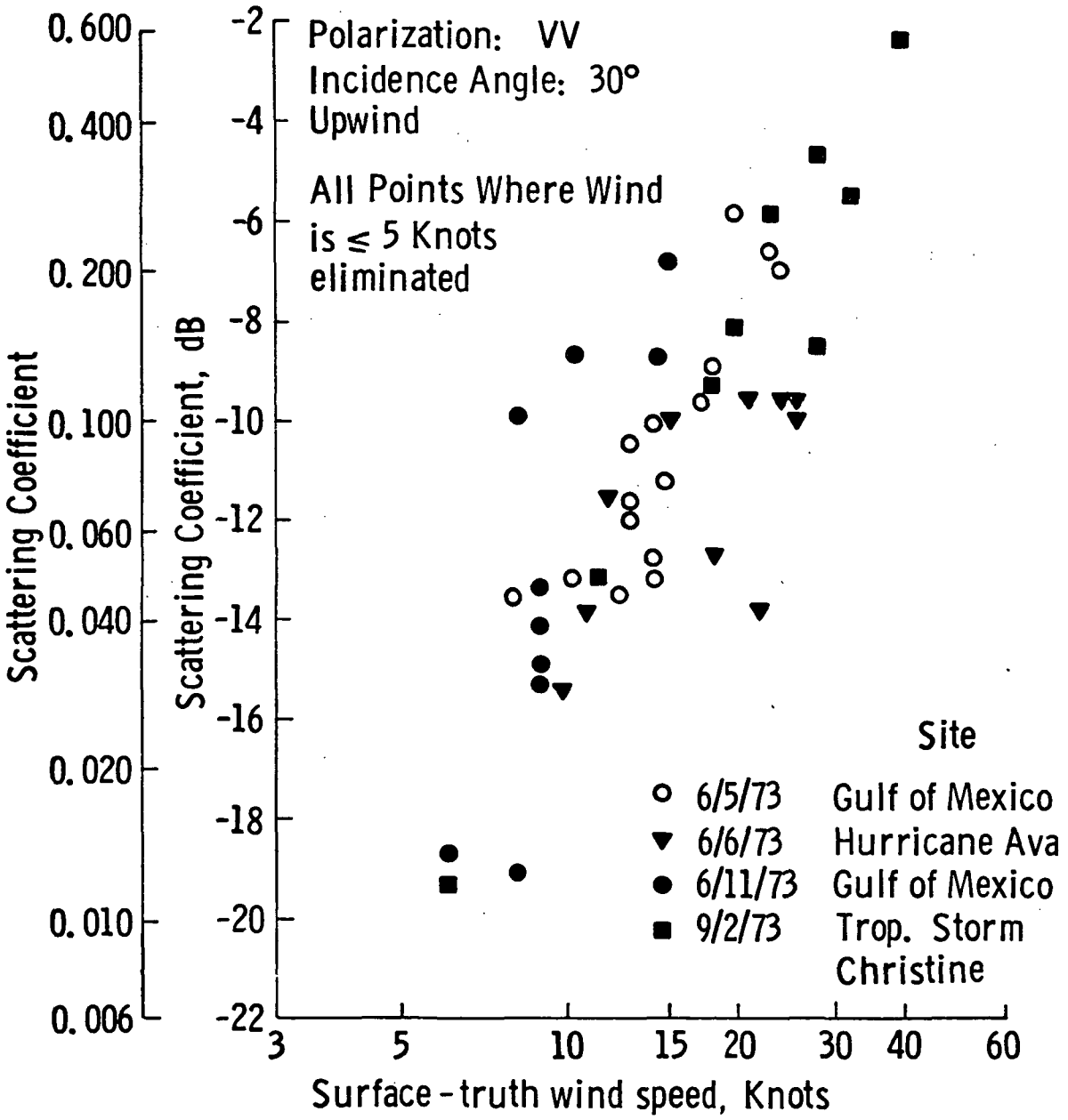

Figure 5a. Wind speed dependence of scattering coefficients (preliminary).

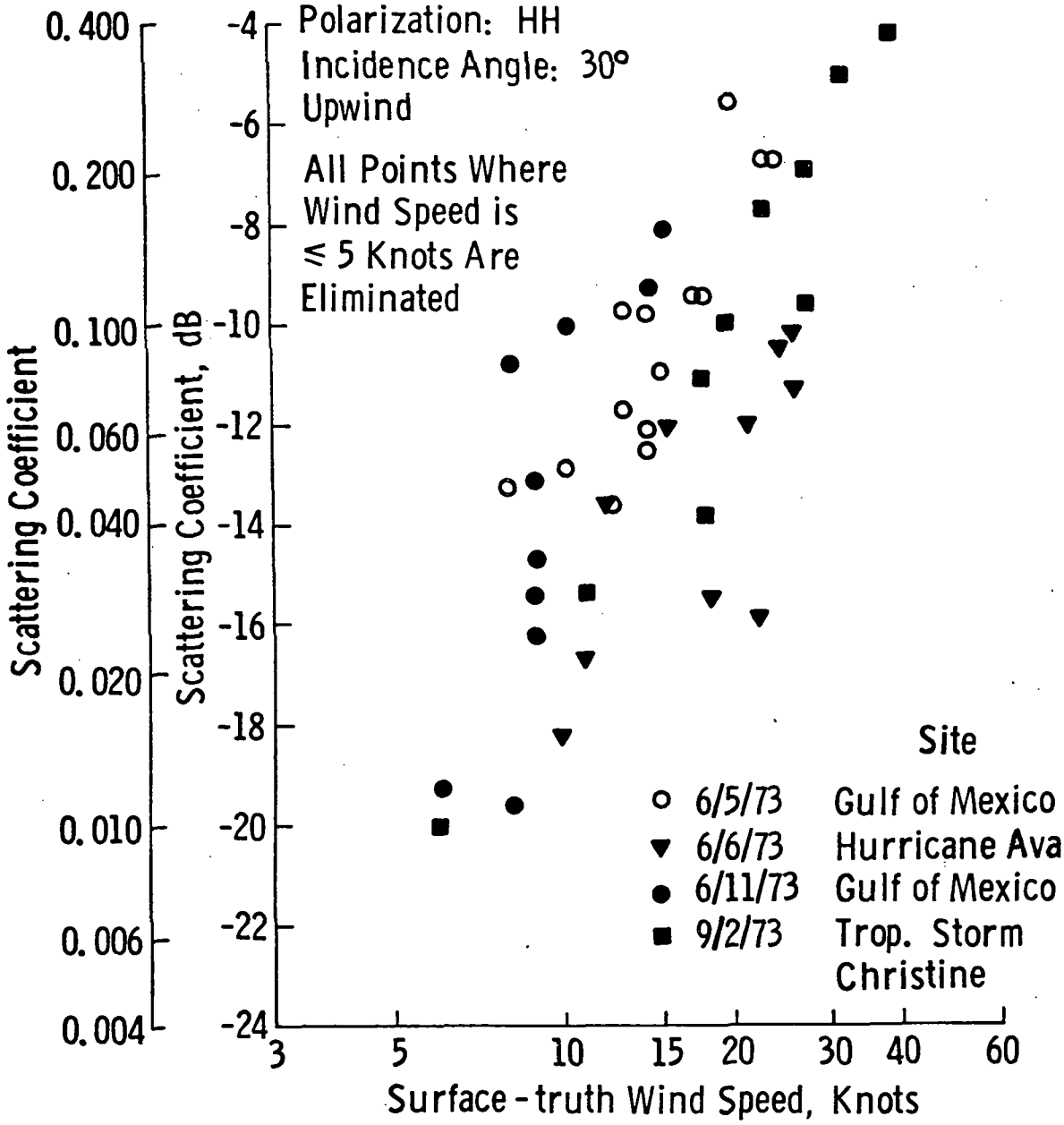

Figure 5b. Wind speed dependence of scattering coefficients (preliminary).

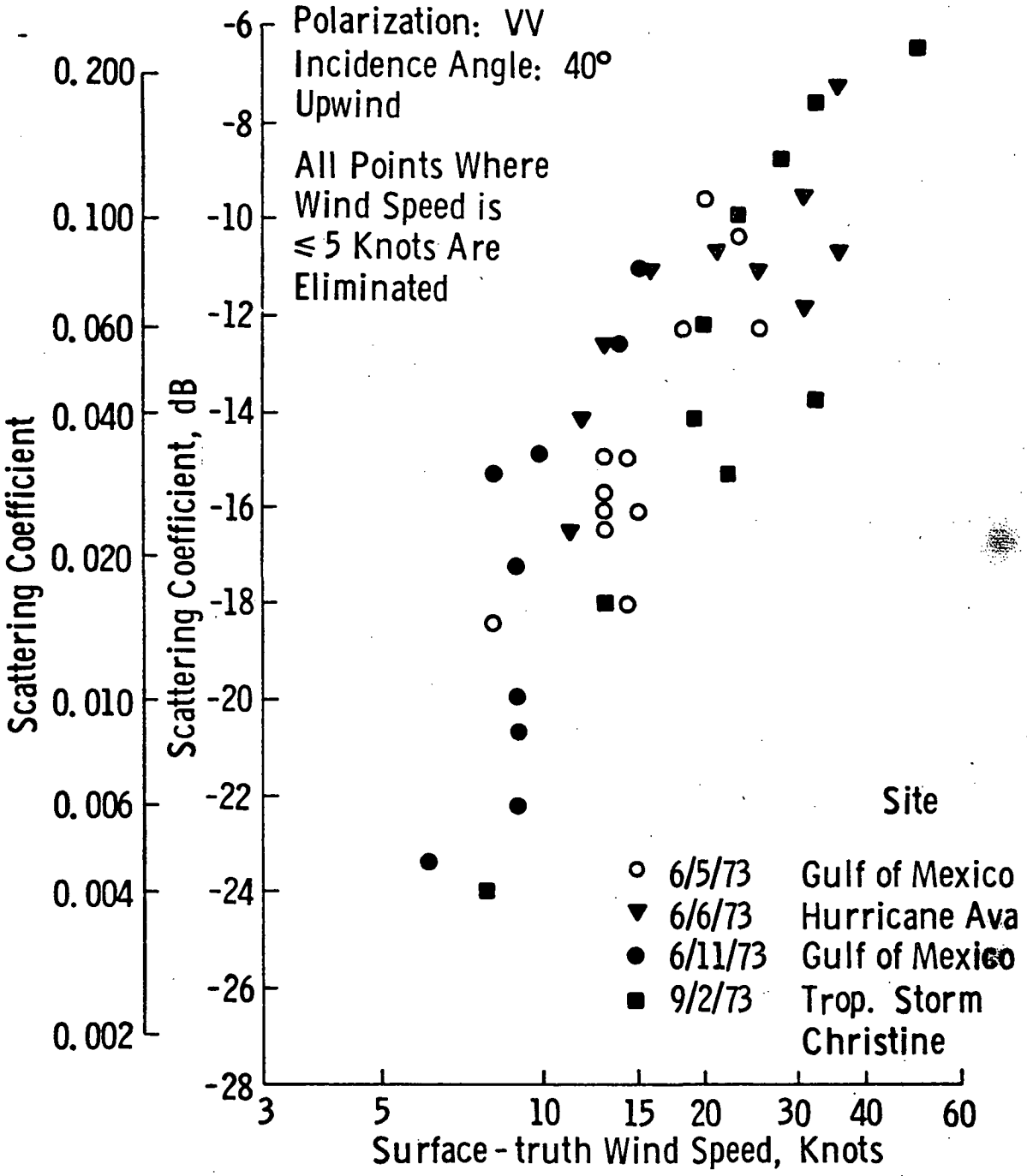

Figure 6a. Wind speed dependence of scattering coefficients (preliminary).

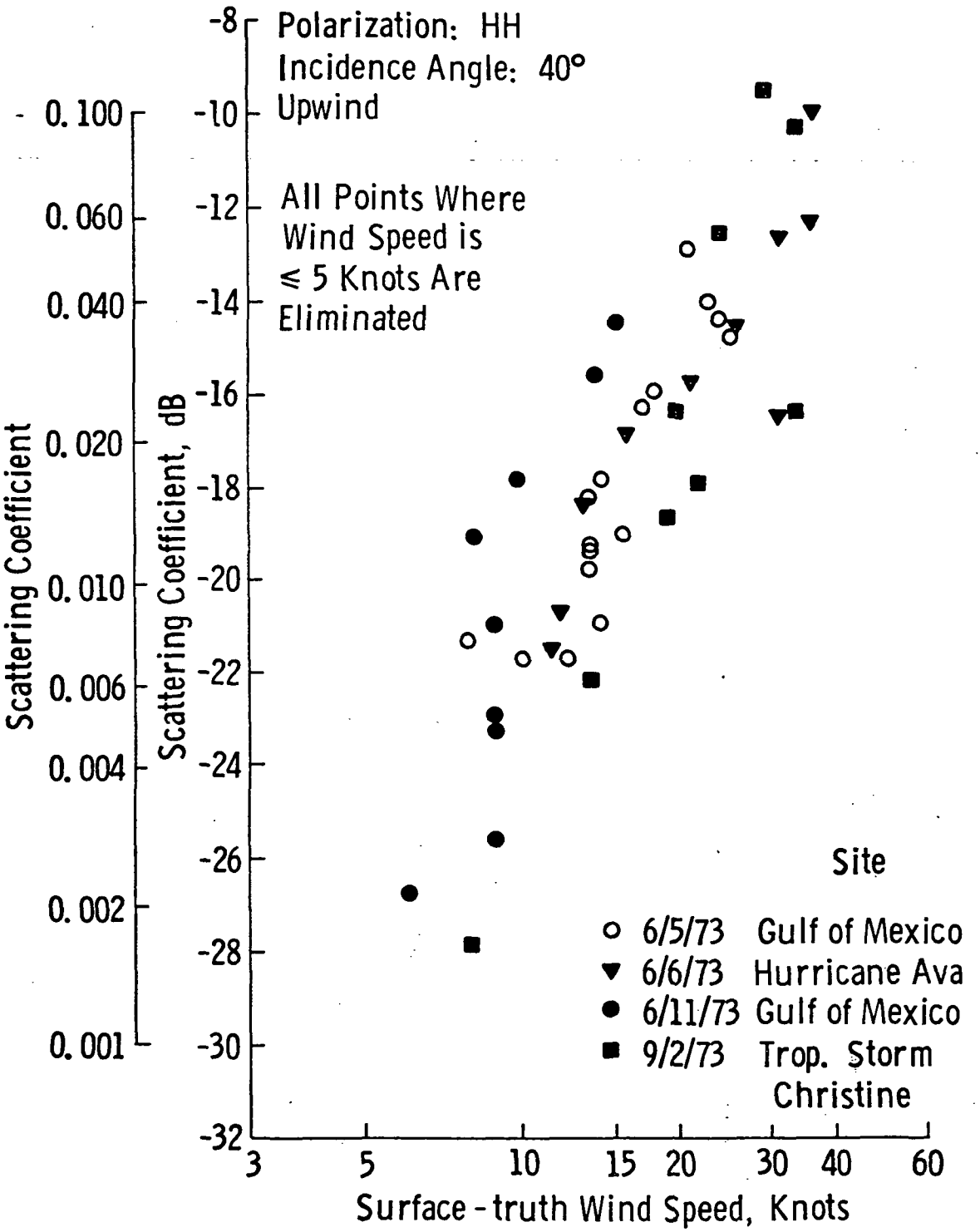

Figure 6b. Wind speed dependence of scattering coefficients (preliminary).

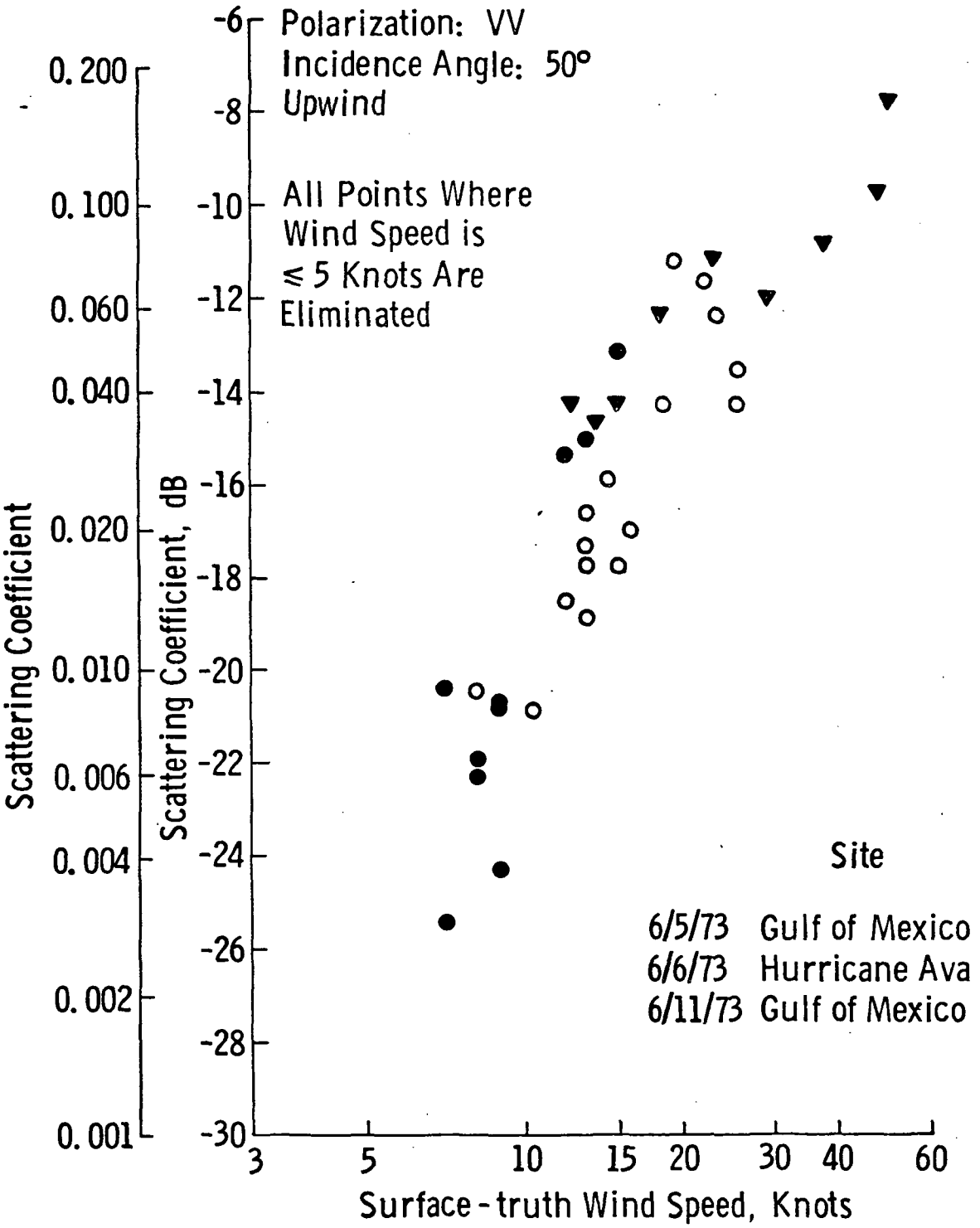

Figure 7a. Wind speed dependence of scattering coefficients (preliminary).

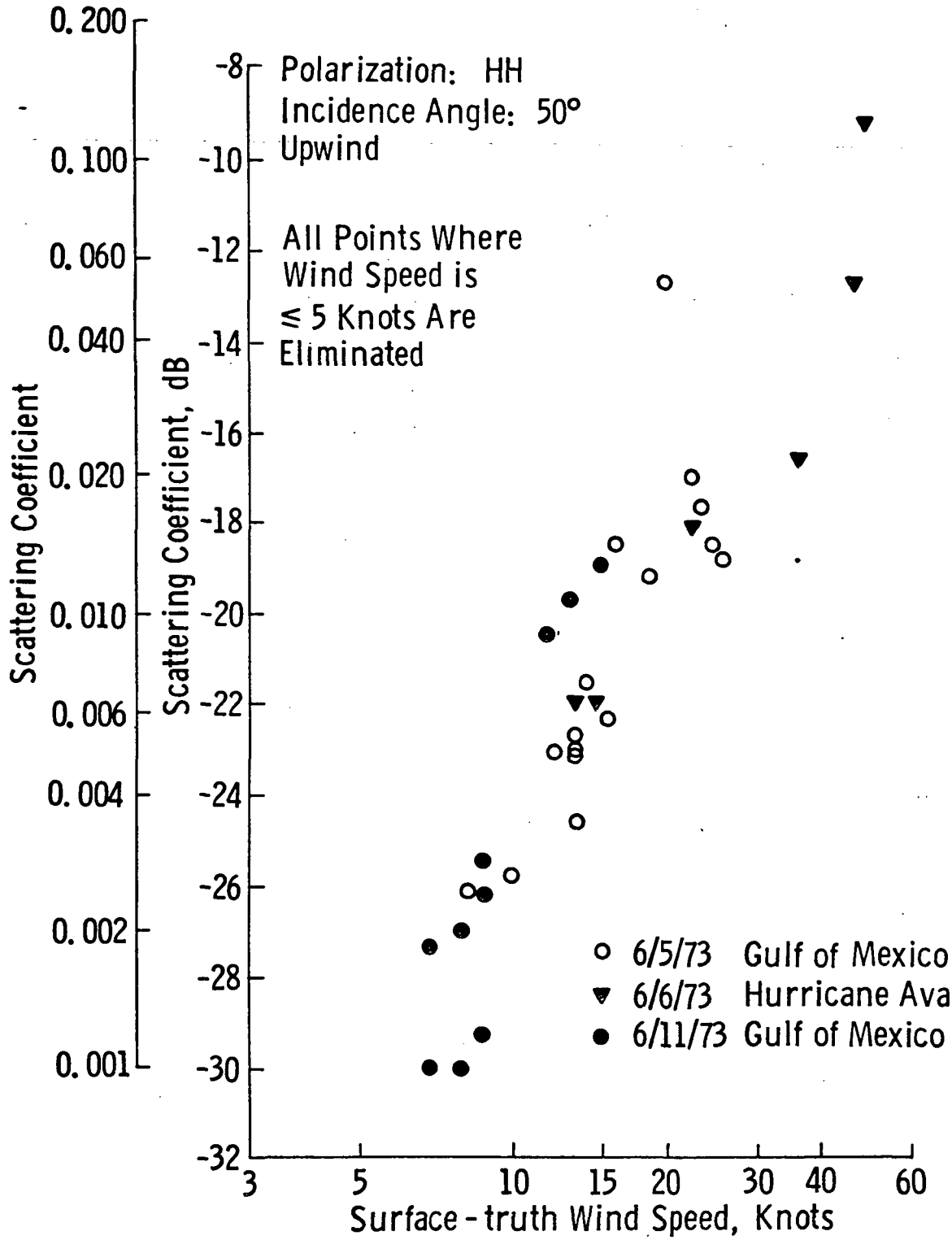

Figure 7b. Wind speed dependence of scattering coefficients (preliminary).

Table 4: Values for parameters A and γ using the theoretical approach to obtain σ^o for vertical polarization

Frequency (GHz) / Cell #	12.5	13.9	15.0
	A/γ (vv)		
1	-17.85 / 1.39	-18.277 / 1.446	-18.671 / 1.488
3	-25.255 / 1.593	-26.143 / 1.670	-26.70 / 1.719
7	-30.669 / 1.761	-31.50 / 1.824	-32.40 / 1.885
12	-34.56 / 1.870	-35.75 / 1.950	-36.684 / 2.012

Table 4 (cont'd.): Values for parameters A and γ using the theoretical approach to obtain σ^o for horizontal polarization

Frequency (GHz) / Cell #	12.5	13.9	15.0
	A/γ (HH)		
1	-19.79 / 1.40	-20.08 / 1.446	-20.471 / 1.488
3	-29.10 / 1.595	-29.795 / 1.656	-30.30 / 1.705
7	-37.18 / 1.755	-38.02 / 1.824	-38.90 / 1.885
12	-44.60 / 1.88	-45.80 / 1.965	-46.484 / 2.012

Table 4 (cont'd.): Values for parameters A and γ using Skylab data (13.9 GHz) for σ^{o} for both vertical and horizontal polarization - Upwind case.*

Polarization / Cell #	vv	HH
	A/γ	
3	-28.91 / 1.536	-29.25 / 1.464
7	-34.43 / 1.680	-39.65 / 1.828
12	-37.79 / 1.833	-46.18 / 2.116

*For the crosswind case A is increased by 4.5 dB.

where

- A = a constant
- U = wind speed
- γ = wind speed power coefficient.

Values for A and γ are given in Table 4 for both theoretical and experimental values of $\sigma_{vv}^{o}(\theta)$ and $\sigma_{HH}^{o}(\theta)$.

To find the error in the measured value of wind speed, $\hat{U}$, the analysis assumes that $\hat{\sigma}^{o}$ (measurement value of σ^{o}) is obtained by measuring the returned power. Using $\hat{\sigma}^{o}$ along with the parameters A and γ, a value for the measured wind speed can be obtained.

$$\hat{u} = 10^{\frac{-A(dB) + \hat{\sigma}_{o}\ (dB)}{10\gamma}} \tag{24}$$

Assuming this is the case, the return power during precipitation will consist of both returns from the ocean and the precipitation.

$$W_{r(s+p)} = W_{rs} + W_{rp} \tag{25}$$

Since the return in precipitation is $W_{r(s+p)}$, the measured value of ocean backscatter, σ^{o}, will now be changed. Thus, an error will occur in the determination of U. Examples of wind speed errors caused by precipitation are given for both upwind and cross wind cases at f = 13.9 GHz in Figures 8, 9, 10, 11 and 12.

Figure 8: (a) Cell 3 at f = 13.9 GHz where both upwind and cross wind cases use SKYLAB value of σ_{vv}^{o} (30°).

(b) Cell 3 at f = 13.9 GHz where both upwind and cross wind cases use SKYLAB value of σ_{HH}^{o} (30°).

Figure 9: (a) Cell 7 at f = 13.9 GHz where both upwind and cross wind cases use SKYLAB value of σ_{vv}^{o} (40°).

(b) Cell 7 at f = 13.9 GHz where both upwind and cross wind cases use SKYLAB value of σ_{HH}^{o} (40°).

Figure 10: Cell 7 at f = 13.9 GHz using the theoretical value of $\sigma_{vv}^{o}(40°)$ and $\sigma_{HH}^{o}(40°)$.

Figure 11: (a) Cell 12 at f = 13.9 GHz where both upwind and cross wind cases use SKYLAB σ_{vv}^{o} (50°).

(b) Cell 12 at f = 13.9 GHz where both upwind and cross wind cases use SKYLAB σ_{HH}^{o} (50°).

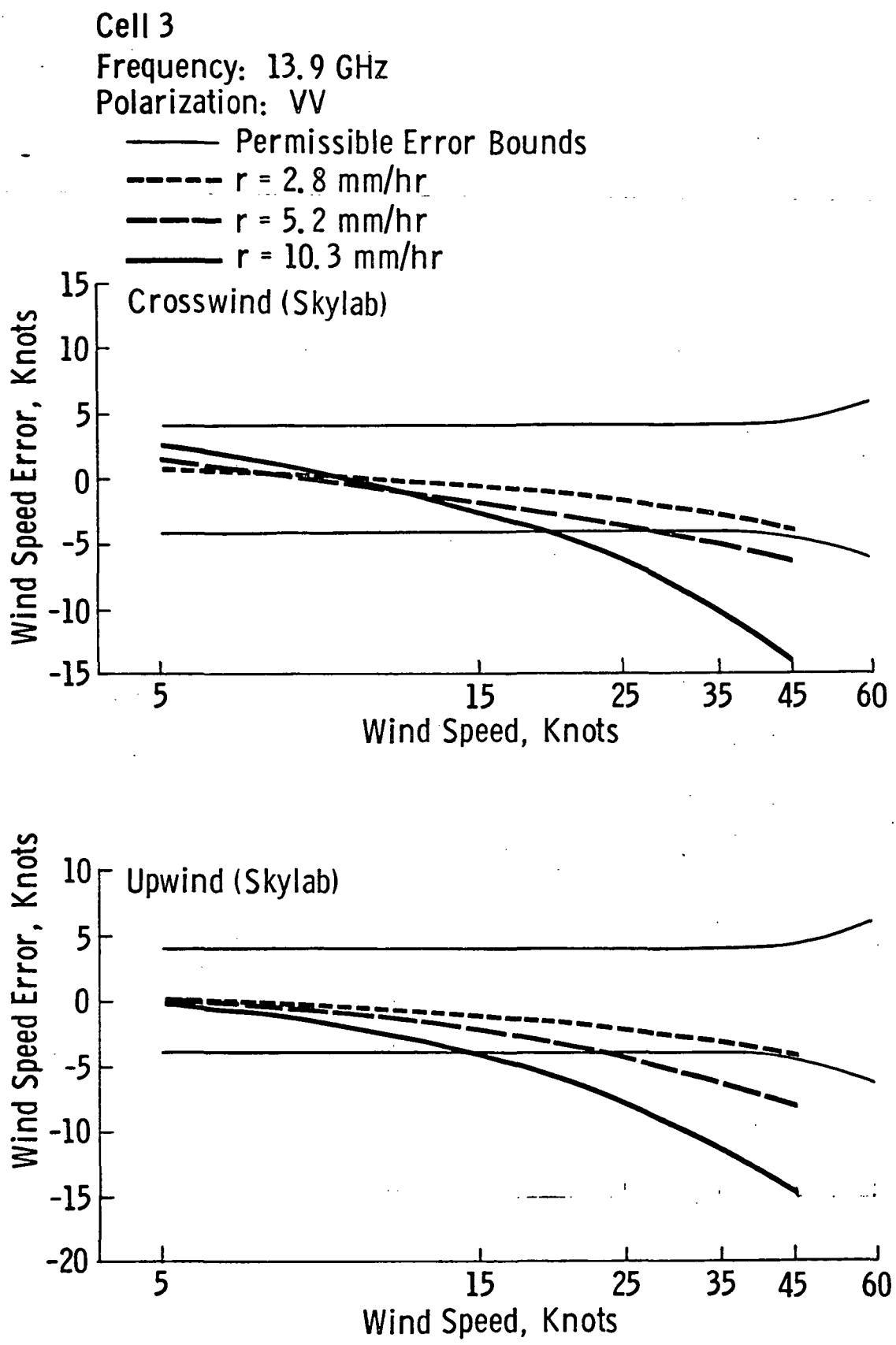

Figure 8a. Wind speed error vs. wind speed.

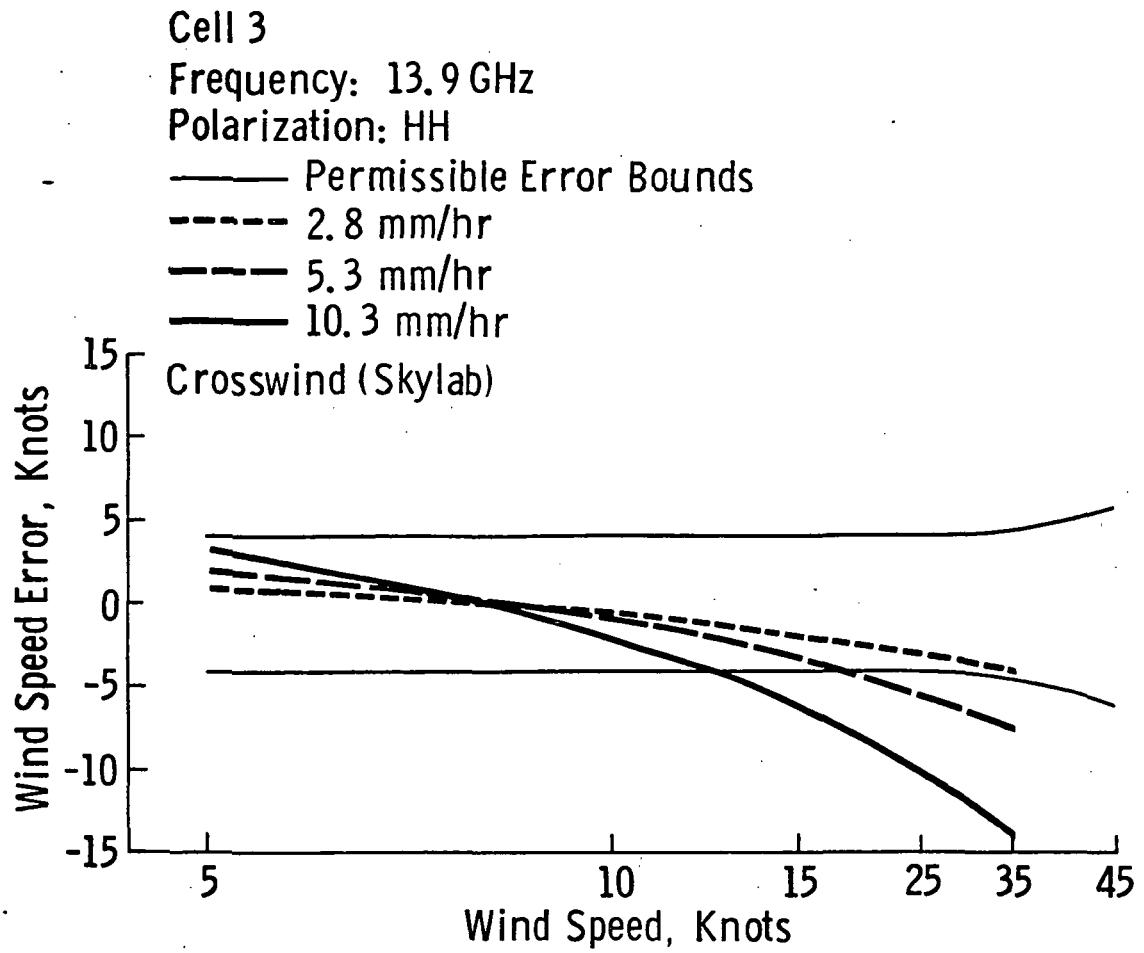

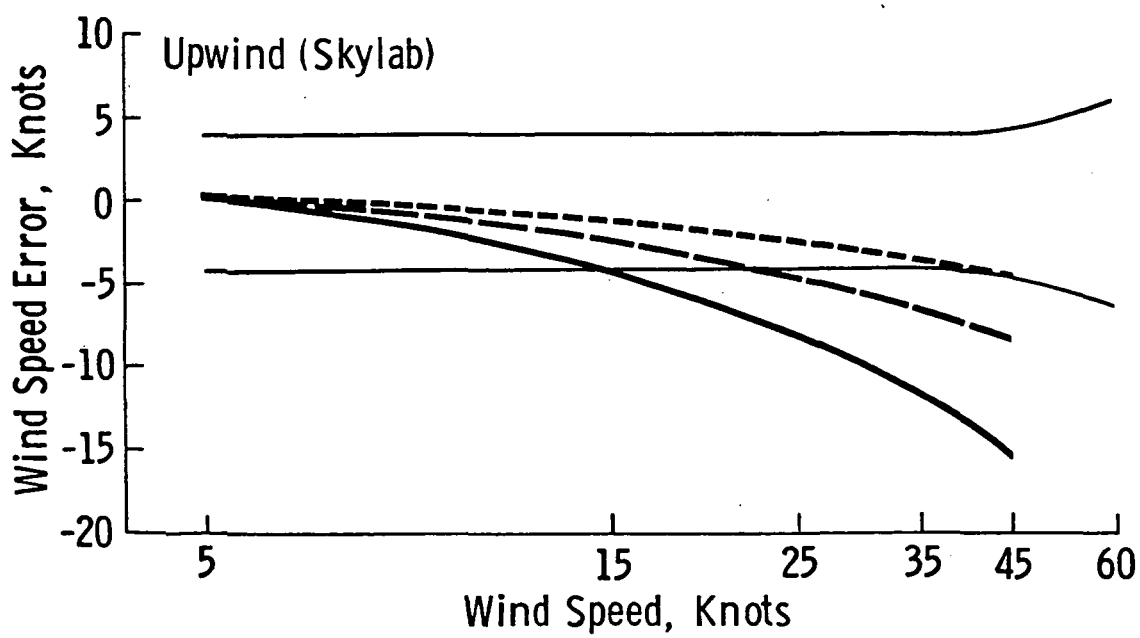

Figure 8b. Wind speed error vs. wind speed.

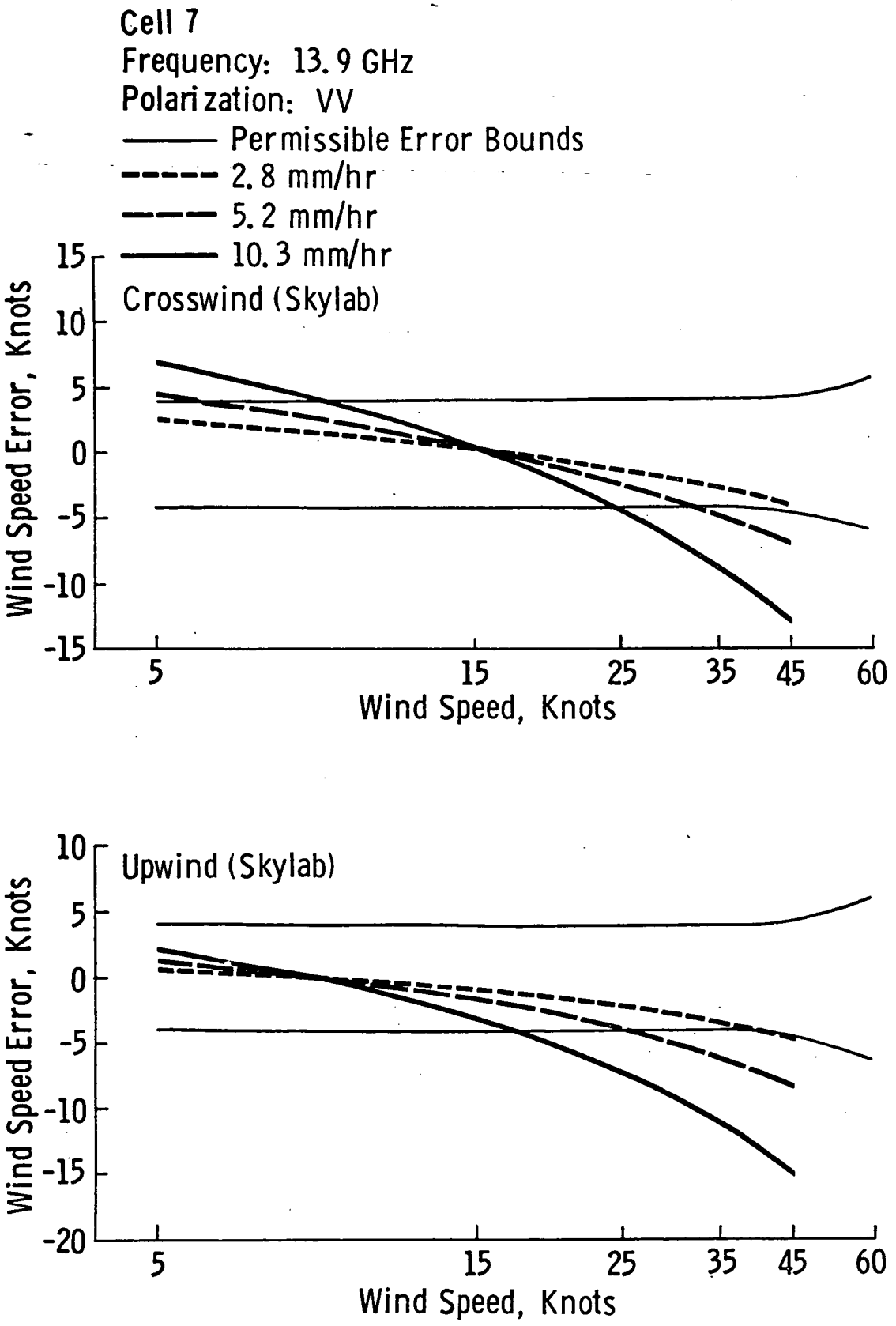

Figure 9a. Wind speed error vs. wind speed.

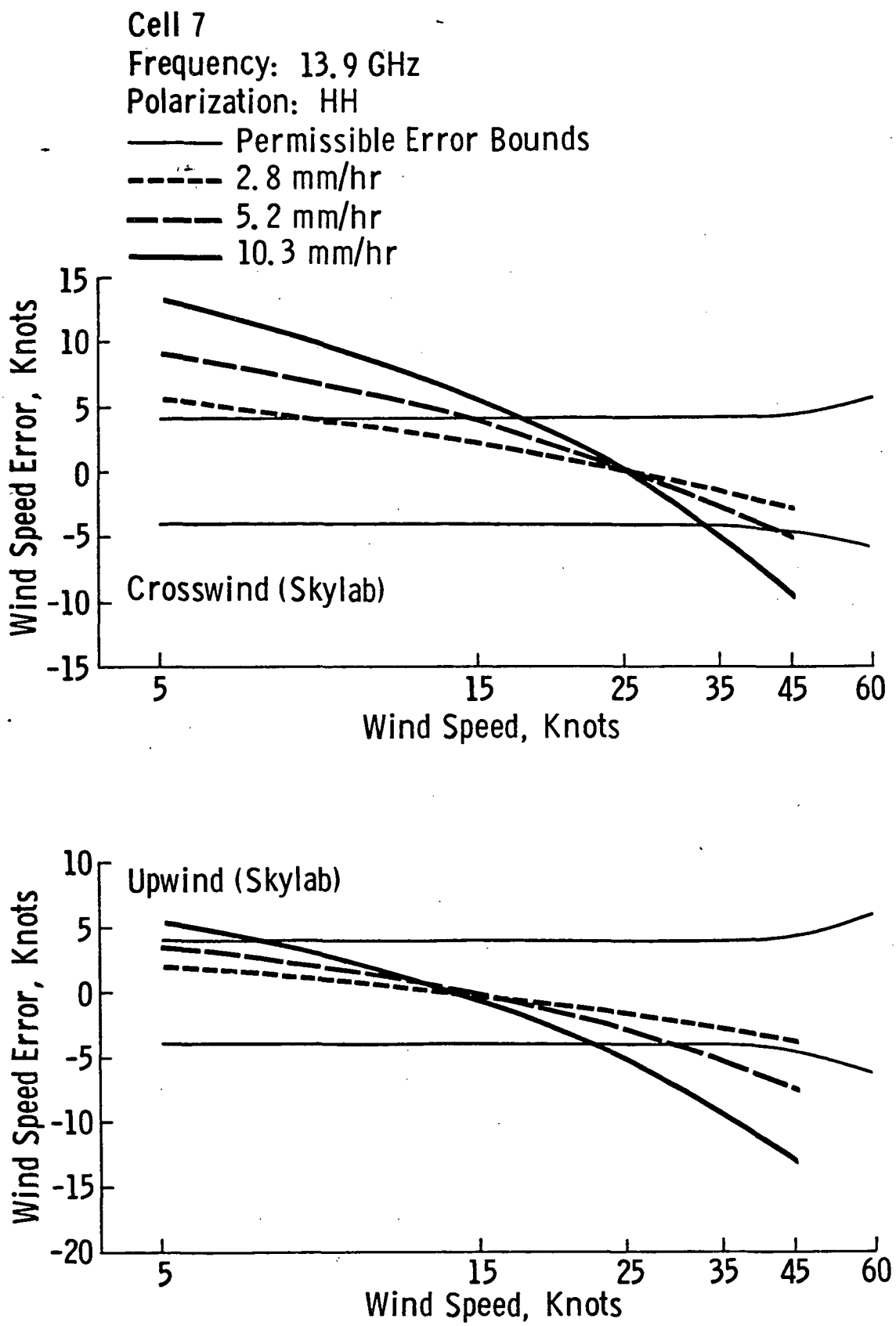

Figure 9b. Wind speed error vs. wind speed.

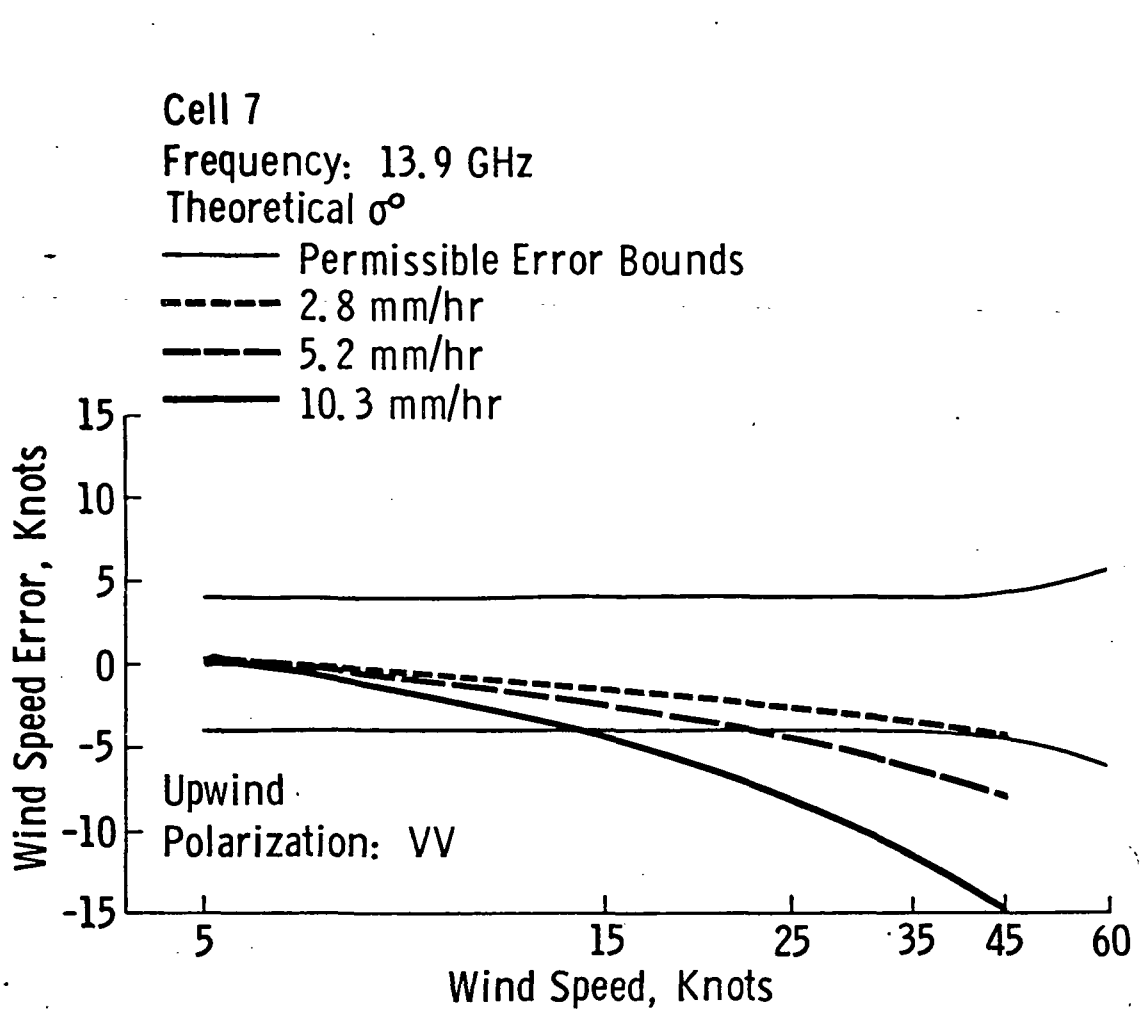

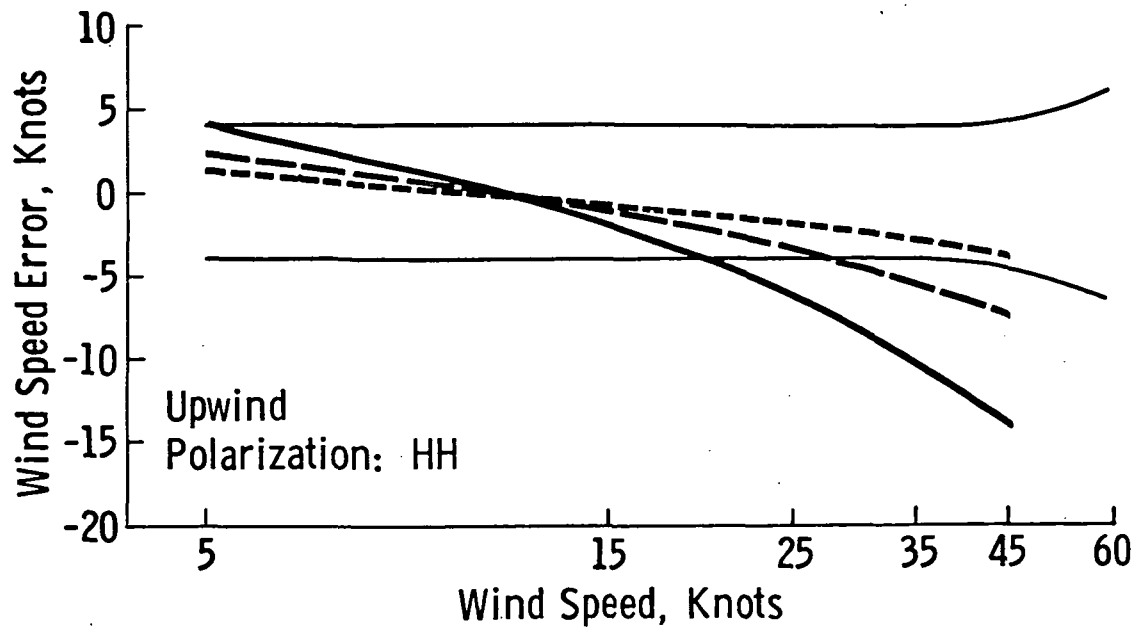

Figure 10. Wind speed error vs. wind speed.

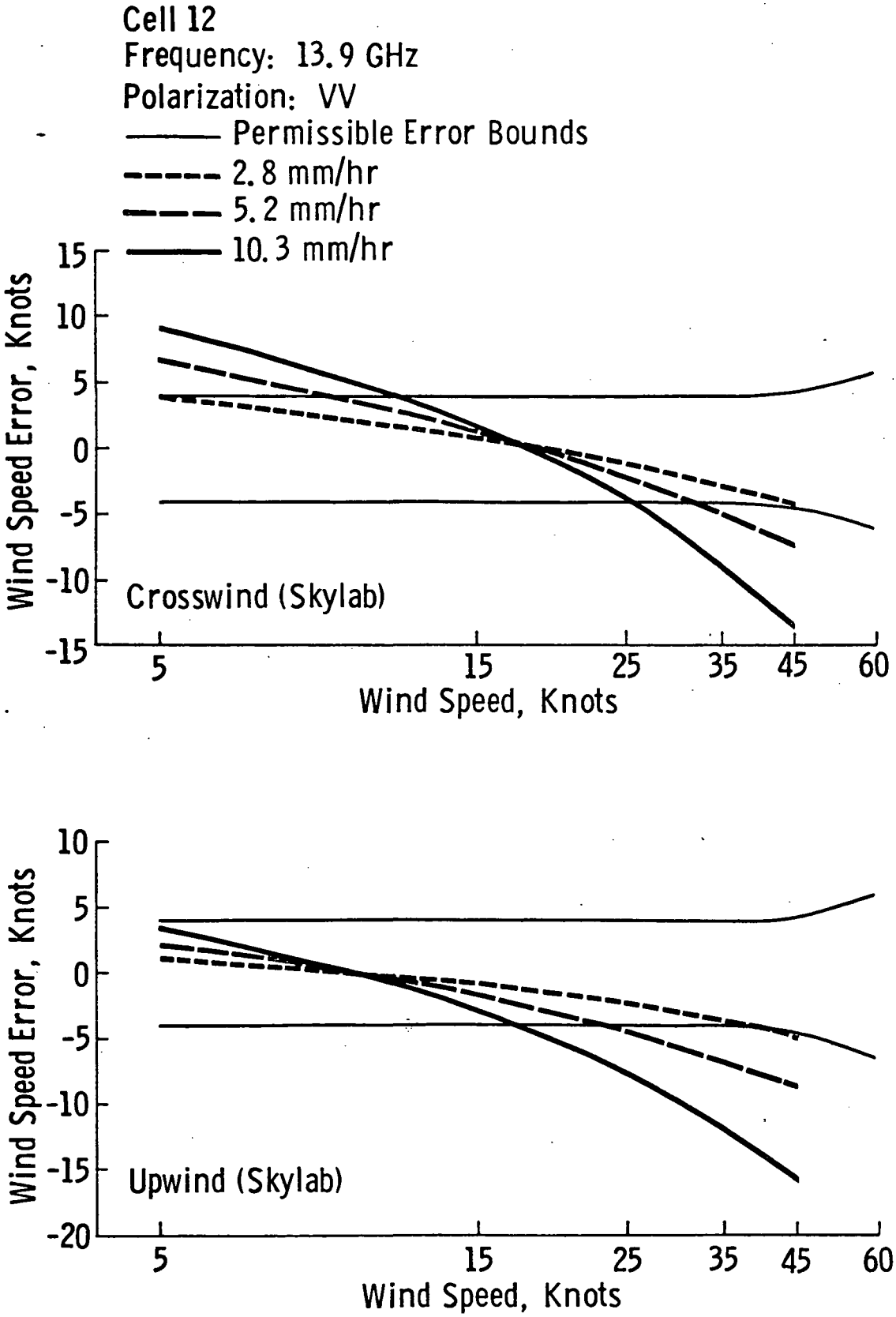

Figure 11a. Wind speed error vs. wind speed.

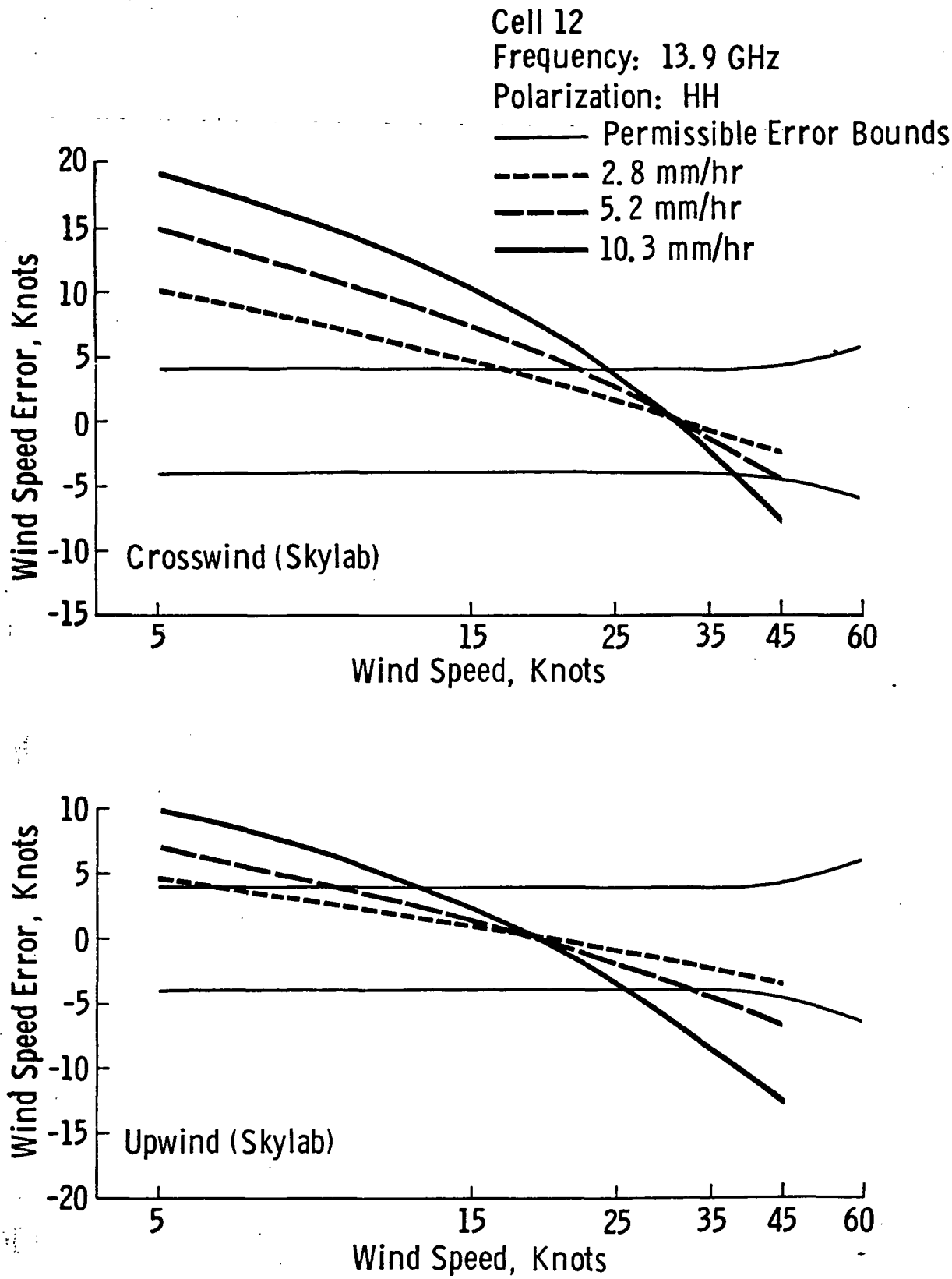

Figure 11b. Wind speed error vs. wind speed.

If a RADSCAT system was used, the radiometer could be used to locate areas of precipitation and to estimate the attenuation.[11] Using the radiometric measurement to correct the scatterometer return would then result in a better estimate of the wind speed. Examples of such corrections are shown in Figures 12a and b.

The original intent of this paper was to determine the degree of improvement realized by operating the scatterometer at lower frequencies where atmospheric effects are less severe. A comparison of wind speed error (due to rain) vs. frequency for the upwind case using the theoretical values of $\sigma_{vv}^{o}(\theta)$ and $\sigma_{HH}^{o}(\theta)$ is shown in Figures 13 - 17.

Figure 13: Cell 7 with wind speed of 5 knots for vv and HH.

Figure 14: Cell 7 with wind speed of 25 knots for vv and HH.

Figure 15: Cell 7 with wind speed of 45 knots for vv and HH.

Figure 16: Cell 12 with wind speed of 5 knots for vv and HH.

Figure 17: Cell 12 with wind speed of 45 knots for vv and HH.

5.0 CONCLUSION

The SEASAT instrument must measure the wind speed to within either $\pm$ 2 m/sec or $\pm$ 10%, whichever is greater to satisfy the user's requirements. Considering only the case where $\sigma_{vv}^{o}(\theta)$ and $\sigma_{HH}^{o}(\theta)$ are determined from SKYLAB data (note, f = 13.9 GHz), it is seen that for the cross wind case:

(1) At cell 3 with vertical polarization this requirement is violated at wind speeds above 45 knots for r = 2.8 mm/hr, wind speeds above 25 knots for r = 5.2 mm/hr, and wind speeds above 18.5 knots for r = 10.3 mm/hr. For horizontal polarization this requirement is violated at wind speeds above 45 knots for r = 2.8 mm/hr, wind speeds above 29 knots for r = 5.2 mm/hr, and wind speeds above 19.5 knots for r = 10.3 mm/hr.

Cell 3

H pol is slightly + in heavy rain not ~ s

(2) At cell 7 with vertical polarization this requirement is violated at wind speeds above 43 knots for r = 2.8 mm/hr, wind speeds of 5 - 9 knots and those above 32 knots for 4 = 5.2 mm/hr, and wind speeds of 5 - 11 knots and those above 25 knots for r = 10.3 mm/hr. For horizontal polarization this requirement is violated at wind speeds of 5 - 17.5 knots for r = 2.8 mm/hr, wind speeds of 5 - 22 knots and those above 44 knots

cell 7

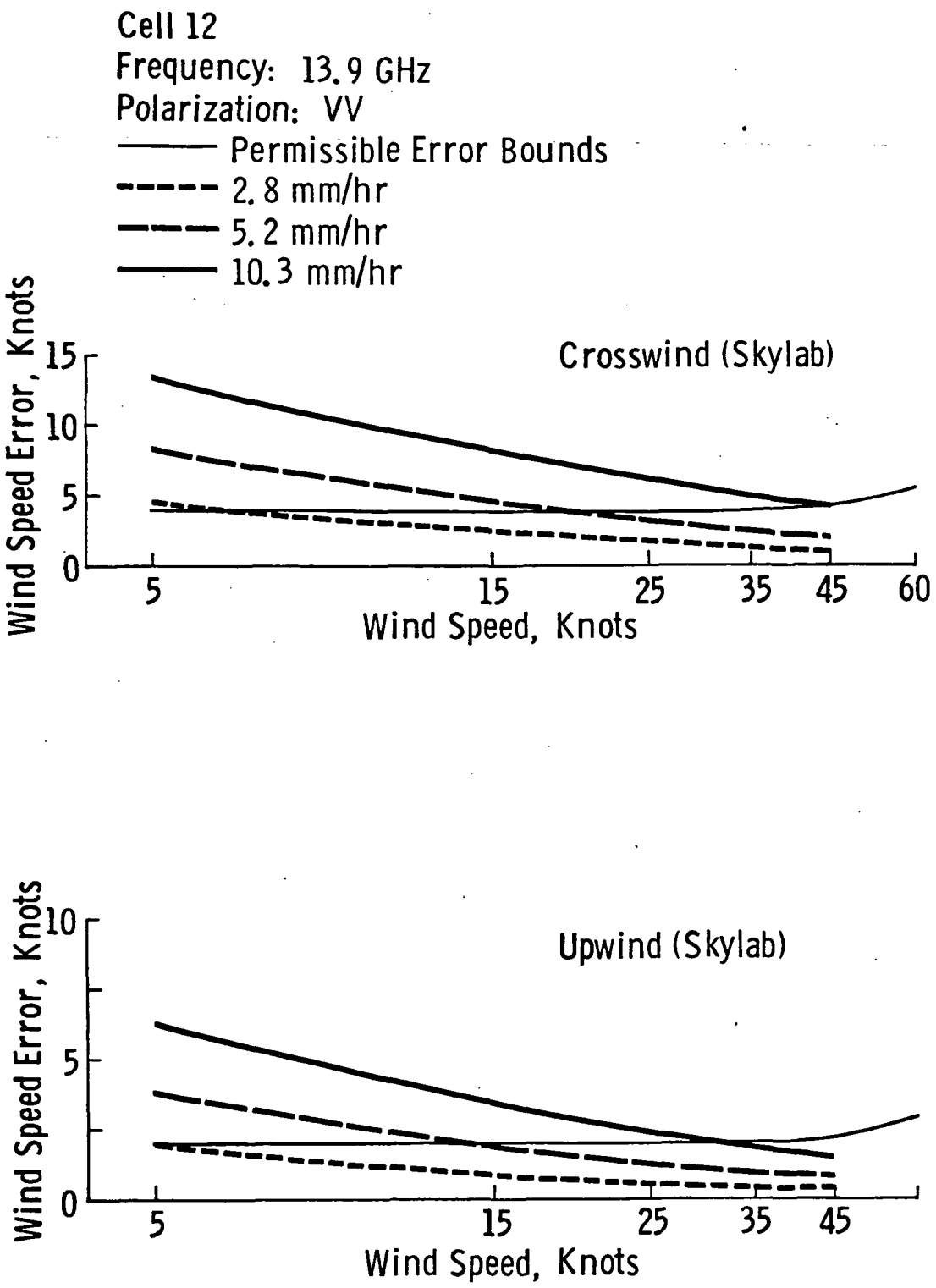

Figure 12a. Wind speed error (when attenuation compensated) vs. wind speed.

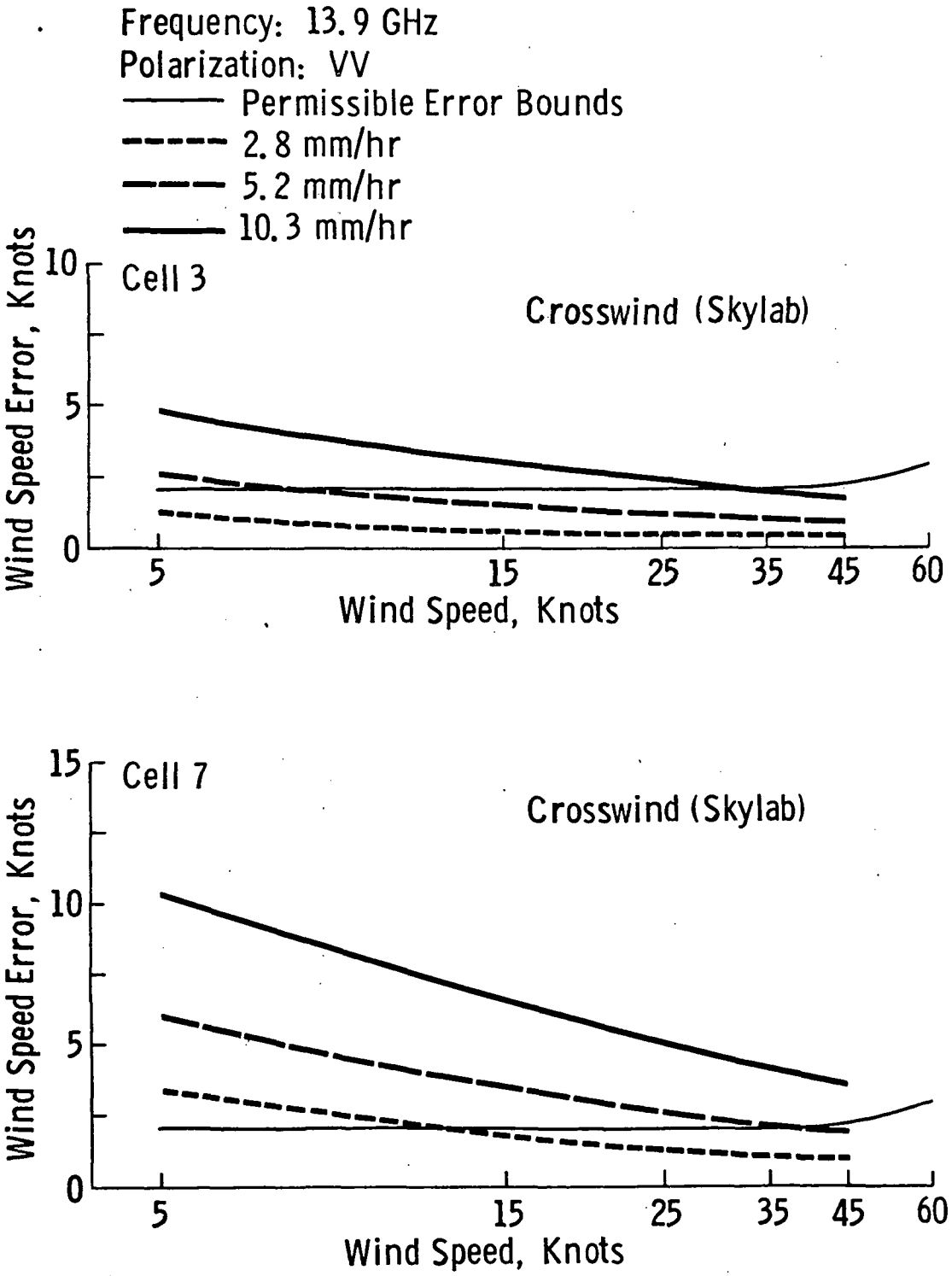

Figure 12b. Wind speed error (when attenuation compensated) vs. wind speed.

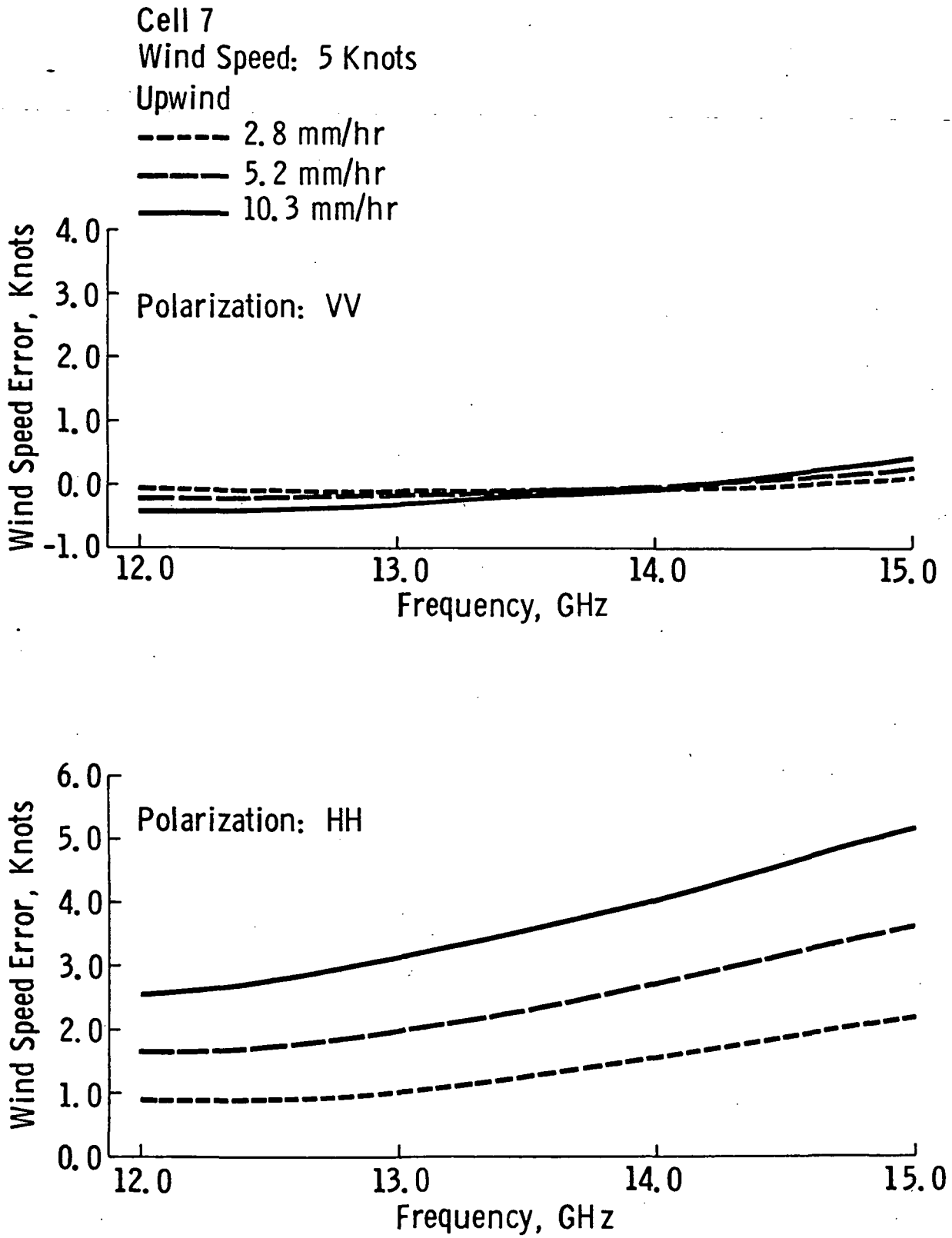

Figure 13. Wind speed error vs. frequency.

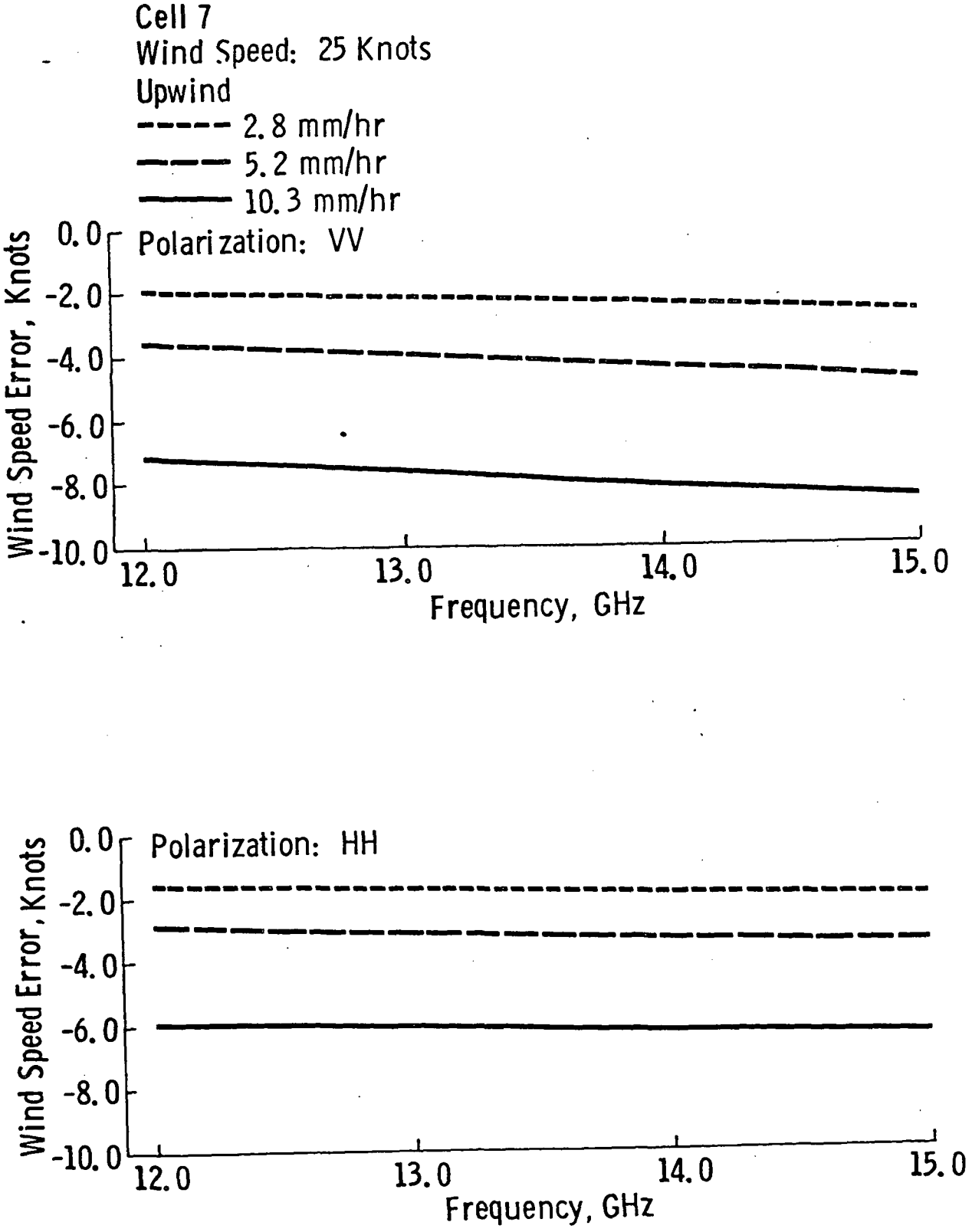

Figure 14. Wind speed error vs. frequency.

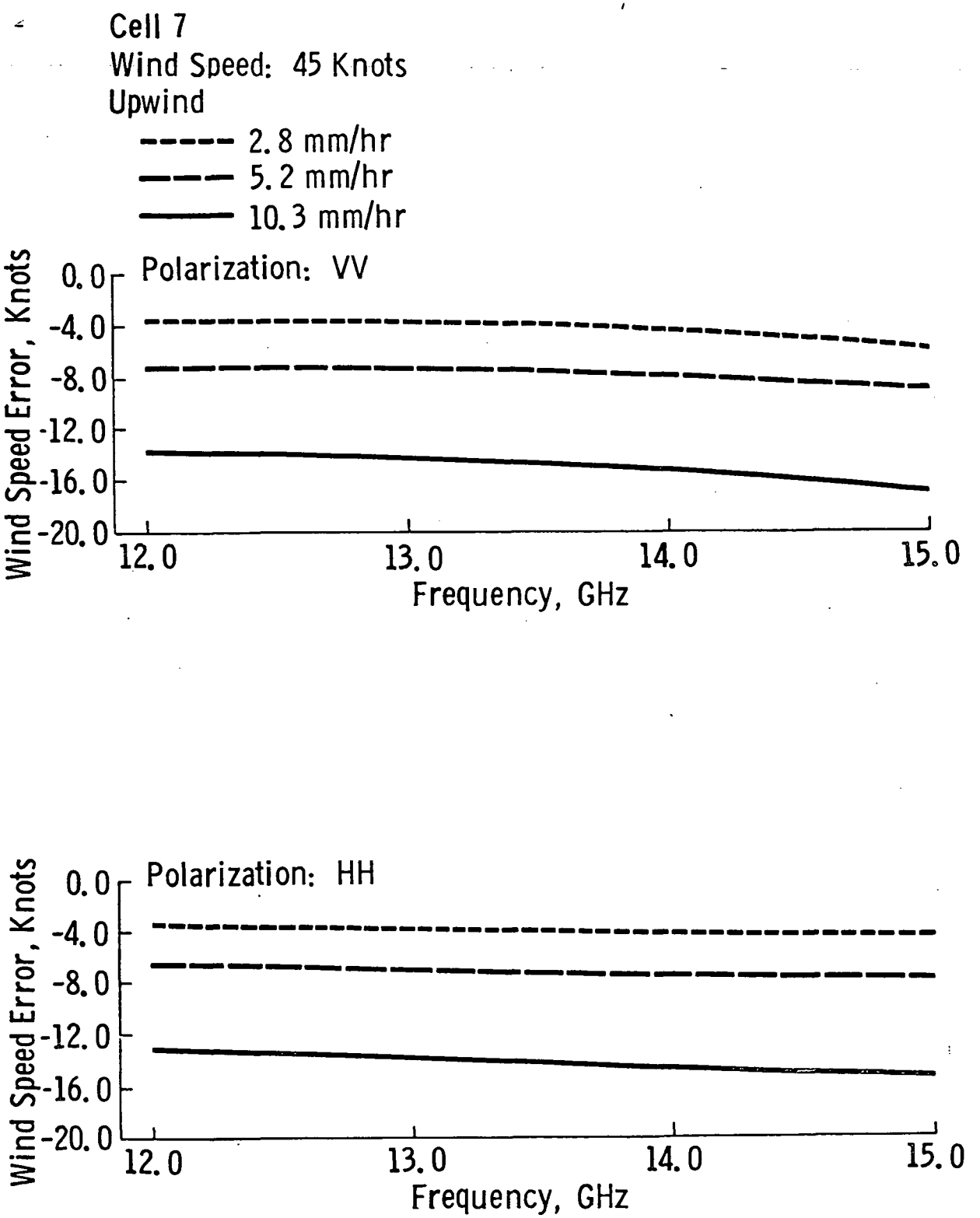

Figure 15. Wind speed error vs. frequency.

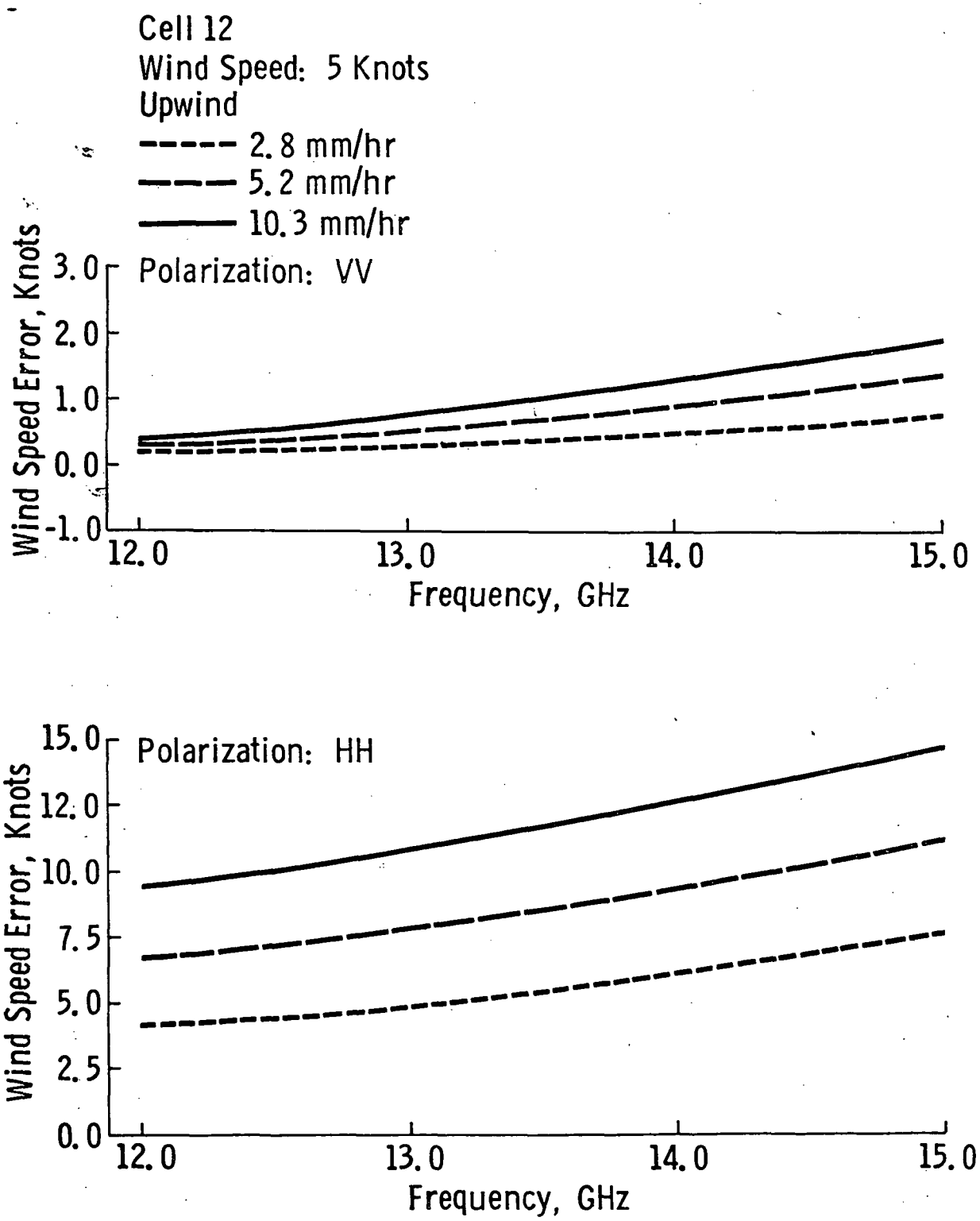

Figure 16. Wind speed error vs. frequency.

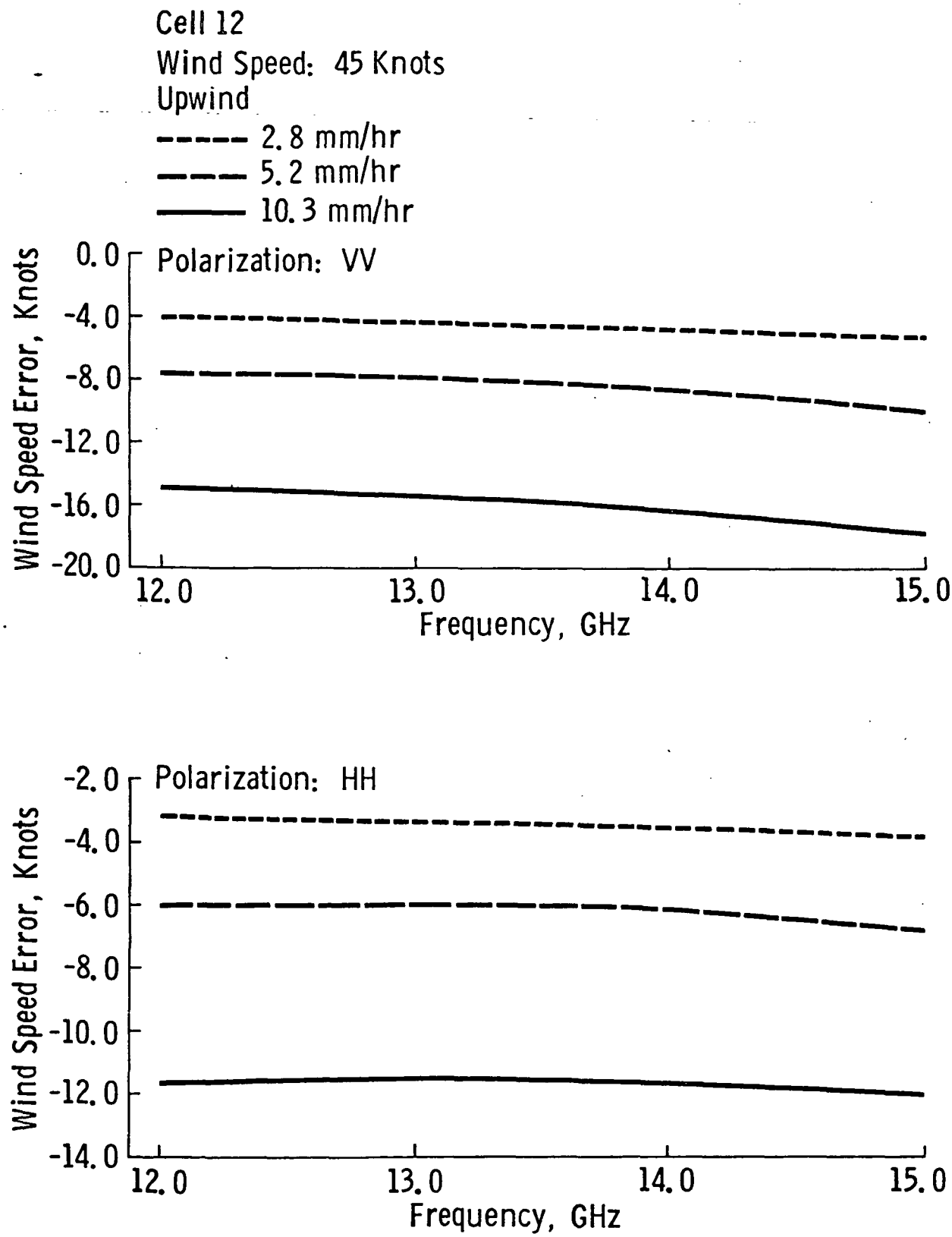

Figure 17. Wind speed error vs. frequency.

for r = 5.2 mm/hr, and wind speeds of 5 - 24 knots and those above 39 knots for r = 10.3 mm/hr.

On the other hand, for the upwind case (again using the SKYLAB results for $\sigma_{VV}^{o}(\theta)$ and $\sigma_{HH}^{o}(\theta)$) it can be seen that:

(1) At cell 3 with vertical polarization the user's requirement is violated at windspeeds above 42 knots for r = 2.8 mm/hr, wind speeds above 23 knots for r = 5.2 mm/hr, and wind speeds above 14 knots for r = 10.3 mm/hr. For horizontal polarization this requirement is violated for wind speeds above 40 knots for r = 2.8 mm/hr, wind speeds above 23 knots for r = 5.2 mm/hr and wind speeds above 14.5 knots for r = 10.3 mm/hr.

(2) At cell 7 with vertical polarization the requirement is violated at wind speeds above 40 knots for r = 2.8 mm/hr, wind speeds above 25 knots for r = 5.2 mm/hr and wind speeds above 17 knots for r = 10.3 mm/hr. For horizontal polarization the requirement is violated for wind speeds above 45 knots for r = 2.8 mm/hr, wind speeds above 30 knots for r = 5.2 mm/hr, and wind speeds of 5 - 6.5 knots and those above 22 knots for r = 10.3 mm/hr.

(3) At cell 12 with vertical polarization the requirement is violated at wind speeds above 39 knots for r = 2.8 mm/hr, wind speeds above 24 knots for r = 5.2 mm/hr, and wind speeds above 17.5 knots for r = 10.3 mm/hr. For horizontal polarization this requirement is violated at wind speeds of 5 - 6 knots for r = 2.8 mm/hr, wind speeds of 5 - 9.5 knots and those above 33 knots for r = 5.2 mm/hr, and wind speeds of 5 - 12.5 knots and those above 26 knots for r = 10.3 mm/hr.

From these results, we can conclude that the wind speed error is governed by two phenomenon: precipitation backscatter and attenuation due to precipitation. Comparing Figure 11a, where both precipitation backscatter and attenuation are present, with Figure 12, where only precipitation backscatter is present, it is possible to separate the wind speed error into two regions where only one effect is dominant. At low wind speeds, the wind speed error is primarily due to precipitation backscatter; whereas, attenuation is the major source of error at high wind speeds.

When the results of Figures 13 - 17 are used to illustrate the frequency effect, in the absence of an attenuation correction, we find:

(1) For upwind 5-knot measurements at Cell 7, all frequencies studied are satisfactory for VV polarization for the three rain rates; but for HH frequencies above 13.9 GHz are unsatisfactory for the 10.3 mm/hr rain rate.

(2) At cell 12, upwind 5-knot VV measurements are all satisfactory; for HH, however, all frequencies are unsatisfactory for r = 5.2 and r = 10.3 mm/hr, and frequencies above 13 GHz are unsatisfactory at 2.8 mm/hr.

(3) For 45 knots upwind at Cell 7, the VV measurements are unsatisfactory above 13.4 GHz for r = 2.8 mm/hr, and for r = 5.2 and 10.3 mm/hr all frequencies are unsatisfactory; the HH measurements are only satisfactory for 2.8 mm/hr and below 13.0 GHz.

(4) For 45 knots upwind at Cell 12, all VV measurements are unsatisfactory; for HH, all 2.8 mm/hr measurements are satisfactory, but measurements at 5.2 and 10.3 mm/hr are unsatisfactory at all three frequencies.

With attenuation corrections, these conclusion would change.

Several other conclusions can be drawn from the results. First, the wind speed error increases as the precipitation rate increases. Second, the error at lower wind speeds increases with incident angle, since the difference between precipitation returns and returns from the ocean becomes larger. Note, at low wind speeds the precipitation return may be larger than the return signal. Third, for higher wind speeds the error does not necessarily increase with increasing incident angles. This unexpected event occurs since the secondary error due to the precipitation return increases with increasing incident angles, thus, cancelling some of the attenuation effect. To see this compare Figures 12a and b with Figures 8a, 9a and 11a, the error due to precipitation backscatter is positive, while the error due to attenuation is negative.

Through the use of a radiometer, the attenuation errors can be minimized. Comparing Figures 12a and b (where the attenuation effect is eliminated) with Figure 8a, 9a, and 11a (where attenuation losses are included) several differences can be distinguished. First, at low wind speeds, where precipitation backscatter is the major source of error, the non-attenuation case experiences greater wind

speed error. As previously mentioned, the errors due to attenuation and precipitation backscatter cancel and thus, the error should increase. Second, the error at high wind speeds for the non-attenuation case is lower. This would be expected, since the major source of error at high speeds, attenuation, is eliminated. Third, for the non-attenuation case, the wind speed error always increases for increasing incidence angles. Fourth, the wind speed error at a particular incident angle decreases with increasing wind speeds for the non-attenuation case.

For the non-attenuation study, as was the case with attenuation study, the wind speed error increases with increasing precipitation rate. Also for low wind speeds, the precipitation return may be greater than the return from the ocean.

The generalized results given so far will apply regardless of how $\sigma_{vv}^{o}(\theta)$ and $\sigma_{HH}^{o}(\theta)$ are determined. As mentioned before, a discrepancy does exist between the theoretical and the empirical values of $\sigma_{vv}^{o}(\theta)$ and $\sigma_{HH}^{o}(\theta)$. An example of this difference is shown in Figures 9 and 10.

Using the theoretical values for $\sigma_{vv}^{o}(\theta)$ and $\sigma_{HH}^{o}(\theta)$ to show the frequency dependence of wind speed error, the following results are obtained: (1) The wind speed error increases as frequency increases; and (2) The wind speed error increases as the rainfall rate increases.

This report may have neglected several areas of possible importance:

(1) The effects of rain on the ocean surface, since this phenomenon has not been studied before;

(2) Some compensation may be available to correct the wind speed error by comparing the horizontal and vertical polarization vertical measurements; and

(3) Use of cross polarization may eliminate or substantially reduce the error caused by precipitation backscatter. Radar meteorologists have long used circular polarization to eliminate the return from spherical particles such as rain.

APPENDIX 1

SEASAT's resolution cell is shown in Figure A.1. To determine the area, first the area of the cell in Figure A.2 is found and then the Doppler effects are subtracted.

The area of the approximate resolution cell (A.2), $A_{CELL'}$, is

$$A_{CELL'} = 2'B' + 'A' \tag{A.1}$$

where

'A' = $\ell \times L'$

'B' = $1/2\ (v_g t_p)\ (\sqrt{2}\, R_c \phi)$

v_g = satellite ground velocity, 6.61 km/sec

t_p = measurement period, 1.891 sec

ϕ = narrow 3 dB beamwidth of the fan beam, 8.73×10^{-3} rad.

R_c = slant range to the center of the doppler cell.

The parameter ℓ is given by

$$\ell = \left[(v_g t_p)^2 + (\sqrt{2}\ R_c \phi)^2\right]^{1/2} \tag{A.2}$$

The value of L' is

$$L' = \sqrt{2} r - \frac{S_s}{8\sqrt{2}} - R_c\, \phi \tag{A.3}$$

where

r = equivalent resolution size

S_s = spacing along the direction of the satellite track between successive scans of the same antenna

R_c = slant range to the center of the cell.

Values of the parameters of $A_{CELL'}$ are given in Table A.1 for cells 1 and 15.

Doppler correction needs to be calculated so that the correct area of the resolution cell, A_{CELL}, can be obtained,

$$A_{CELL} = A_{CELL'} - 2A_d \tag{A.4}$$

where A_d, the area lost by Doppler shift, is shown in Figure A.3. Values of the angles and area of the Doppler correction are given in Table A.2.

Table A.1: Parameters of $A_{CELL'}$ for cells 1, 3, 7, 12

Cell #	(km)	'A' (km^2)	'B' (km^2)	$A_{CELL'}$ (km^2)
1	16.53	896.26	67.57	1031.40
3	17.09	916.54	72.81	1062.16
7	18.72	973.63	87.06	1147.75
12	21.48	1265.39	109.19	1483.77

Table A.2: Values of the various angles and $A_{Doppler}$ need for doppler correction

Cell	A	B	C	h	b	$A_{Doppler}$
1	84.99	50.01	39.99	0.94	11.89	5.59
3	81.05	53.95	36.05	1.81	14.00	12.67
7	72.01	62.99	27.01	4.30	21.68	46.61
12	62.62	72.38	17.62	8.03	40.79	163.77

Recalling (A.4), it is now possible to calculate the correct cell area.

$A_{CELL\ 1} = 1031.4 - 2(5.59) = 1020.22$

$A_{CELL\ 3} = 1062.16 - 2(12.67) = 1036.82$

$A_{CELL\ 7} = 1147.75 - 2(46.61) = 1054.53$

$A_{CELL\ 12} = 1483.77 - 2(163.77) = 1156.23$

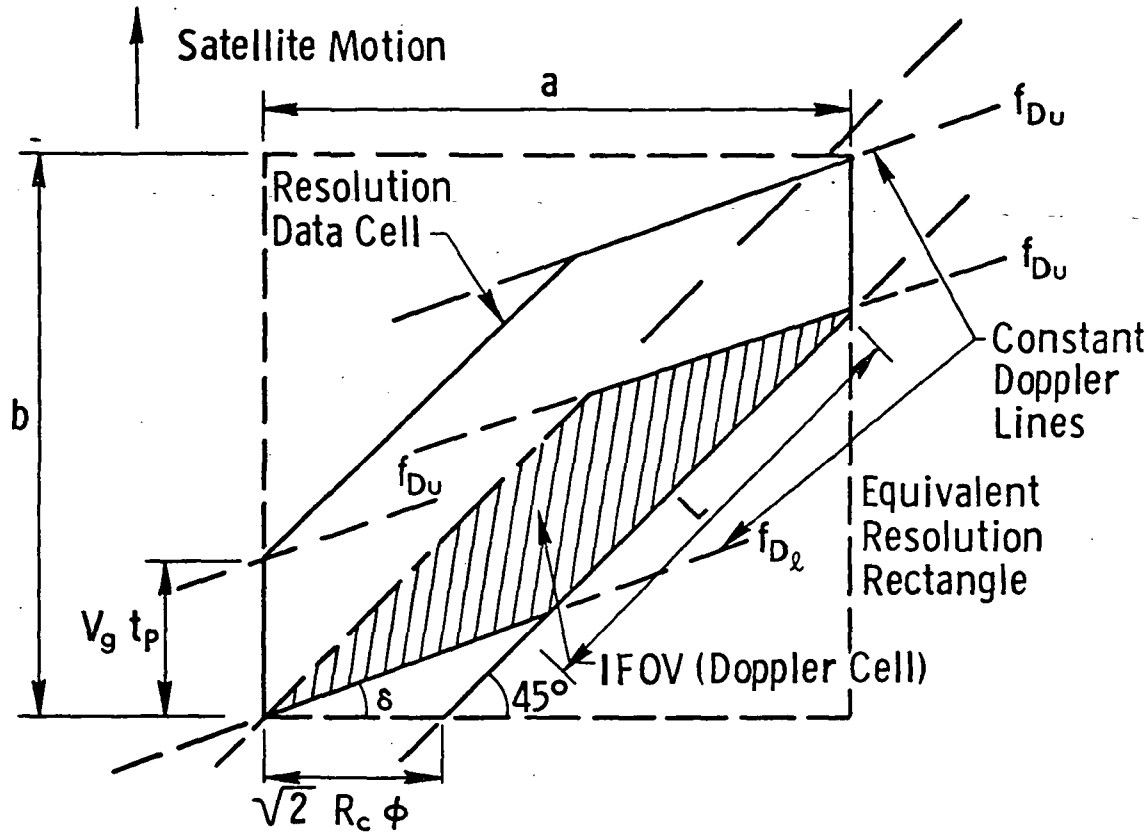

Figure A.1: SEASAT's resolution cell.

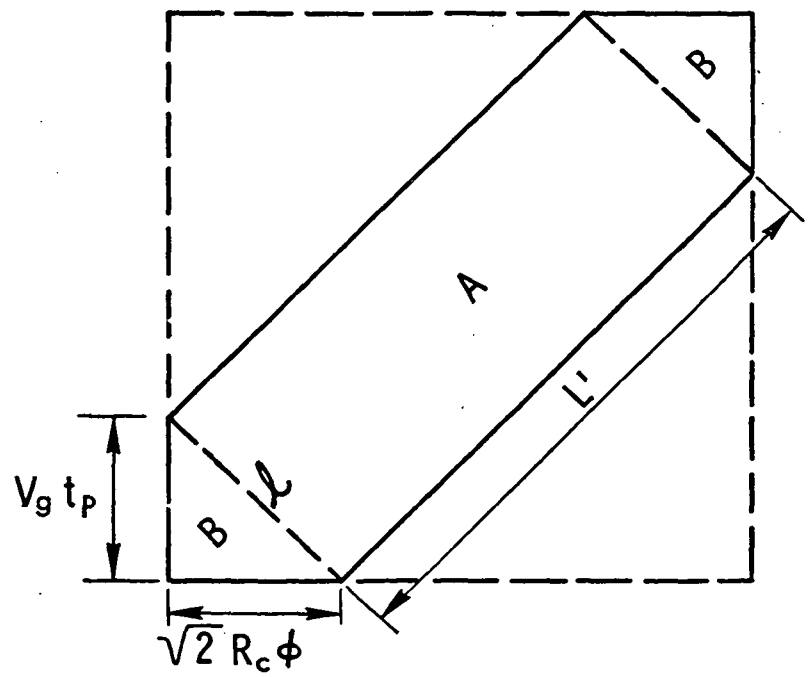

Figure A.2: Approximate resolution cell.

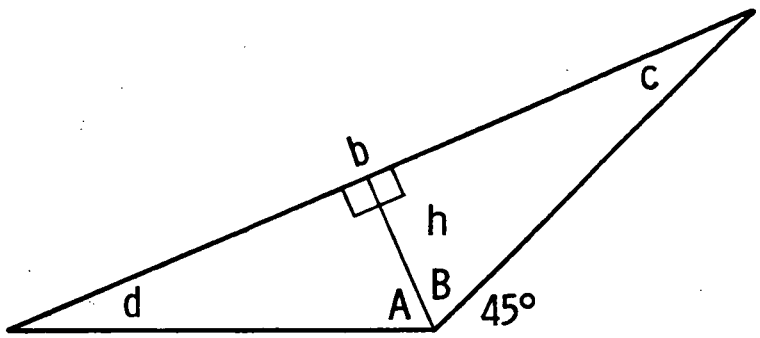

Figure A.3:

REFERENCES

1. Battan, L.J., "Radar Meteorology," University of Chicago Press, Chicago, 1959.

2. Medhurst, R.G., "Rainfall Attenuation of Centimeter Waves: Comparison of Theory and Measurement," IEEE Trans. on Ant. and Prop., vol. AP-13, July 1965, pp. 550-564.

3. Valley, S.L., "Handbook of Geophysics and Space Environment," McGraw-Hill Book Co., New York, 1965.

4. Holzer, W., "Atmospheric Attenuation in Satellite Communications," The Microwave Journal, vol. 8, no. 3, pp. 119-125, March 1965.

5. Pierson, W.J., Jr., Private communication.

6. Chan, H.L. and A.K. Fung, "Backscatter from a Two-Scale Rough Surface With Application to Radar Sea Return," NASA CR-2327.

7. Porter, R.A. and F.J. Wentz III, "Microwave Radiometric Study of the Ocean Surface Characteristics," Final Report, Radiometric Technology, Inc., Wakefield, Mass., July 1971.

8. Grantham, W.L., E.M. Bracalenk, W.L. Jones, J.H. Schrader, L.C. Schroeder, J.L. Mitchell, "An Operational Satellite Scatterometer for Wind Vector Measurements Over the Ocean," Working document at Langley Research Center.

9. Ippolito, Louis J., "Millimeter Wave Propagation Measurements from the Applications Technology Satellite (ATS-V)," IEEE Trans. on Ant. and Prop., vol. AP-18, July 1970, pp. 335-552.

10. Ippolito, Louis J., "Earth-Satellite Propagation Above 10 GHz," Papers from the 1972 URSI Session on Experiments Utilizing the ATS-5 Satellite, X-751-72-208, May 1972.

11. Moore, Richard K. and F.T. Ulaby, "The Radar Radiometer," Proceedings of the IEEE, vol. 57, no. 4, April 1969.